High-Temperature Metal / Molten Alkali Carbonate Interfaces: a Molecular Dynamics Study

D. L. Roest(1), P. Ballone(1,2,3), D. Bedeaux(1), S. Kjelstrup(1) †

(1) Department of Chemistry, Norwegian University
of Science and Technology (NTNU), 7491 Trondheim
(2) Department of Physics, Norwegian University of
Science and Technology (NTNU), 7491 Trondheim and
(3) Italian Institute of Technology, Via Morego 30, 16163 Genova, Italy

Abstract

Interfaces between molten carbonates M_2CO_3 (M=Li, Na and K) and planar metal walls have been investigated by molecular dynamics based on a rigid-ions force field (Janssen and Tissen, Mol. Simul. **5**, 83-98, (1990)). Simulations cover the temperature range 1200 K $\leq T \leq$ 1500 K at a moderate ($\sim$ 15 kbar) overpressure to compensate for a slight overestimate of the system volume by the force field model. Most of the simulations represent neutral electrodes, but shorter computations have been carried out for systems with a low surface charge distribution on the metal side of the interface. The results provide an intriguing view of the interplay among ion packing, oscillating screening, anisotropic correlations and ion dynamics at the interface. The mass and charge density profiles display prominent peaks at contact, and tend to their constant bulk values through several oscillations, whose amplitude decays exponentially moving away from the interface. Oscillations in the charge density profile, in particular, limit the value of the interfacial dipole, and increase the capacitance of the interface. Ion-ion correlations are enhanced in proximity of the metal surface, but retain the exponentially-decaying oscillatory form of their bulk counterpart. Diffusion is slower in the molecularly thin layer of ions next to the interface than in the bulk. The analysis of interfaces is completed by the computation of structural properties of bulk phases, and by the estimate of transport coefficients such as self-diffusion, electrical conductivity, and especially thermal conductivity, which is seldom computed by simulation. All together, the results of our simulations for homogeneous and inhomogeneous molten carbonates provide crucial insight on systems and properties relevant for advanced devices such as fuel cells, that, in turn, might play a prominent role in future power generation strategies.

I. INTRODUCTION

The textbook picture of ionic liquids and solids primarily concerns single-atom ions, and, in this acception, ionic systems have been modelled[1] and simulated[2–4] at the atomistic level since a few decades ago. The present research activity, however, is focused on molecular ionic systems, as highlighted by the overwhelming interest for the so-called room temperature ionic liquids (RTILs[5]), driven by potential applications requiring ionic conductors liquid down to low temperature ($T \sim 300$ K) and chemically stable up to at least $T \sim 600$ K.

Carbonate salts are an important and fairly extended class of molecular ionic compound, relevant, first of all, for mineralogy,[6,9] geophysics[7,8] and even environmental sciences, since geological formations made of limestone ($CaCO_3$) are the most apparent manifestation of massive biomineralisation processes, affecting the global carbon cycle over geological time scales.

The small size and relatively low complexity of the carbonate ion make metal-carbonates closer to traditional salts like NaCl or $MgCl_2$ than to organic ionic system such as RTILs.[10,11] The melting temperature of carbonates of simple monovalent metal ions, for instance, is comparable to that of alkali-halides.[10] Since the carbonate anion is di-valent, however, a fair comparison is with M_2X compounds such as Li_2O, or Na_2O, whose melting temperature is still significantly higher.

Nevertheless, the low viscosity, high ionic conductivity, chemical stability, wide availability and low environmental impact make molten carbonates important players in high temperature fluid technology, with applications in heat transport and thermal energy storage. In economic terms, however, the brightest outlook for carbonate technologies concerns electrochemistry, with applications in molten carbonate fuel cells (MCFC)[12,13,50,51] and in high capacity rechargeable batteries.[14] Molten carbonate fuel cells, moreover, can be coupled to CO_2 capture and sequestration stages,[15,16] enhancing the efficiency and the environmental appeal of these devices. Many other applications are being considered, including recent attempts to develop efficient thermoelectric energy converters based on ionic conductors,[17] and the usage of molten alkali-carbonates as the solvation medium for photovoltaic processes powered by concentrated solar radiation.[18]

In most of these applications, the liquid carbonate interface with a conducting electrode is an essential part of the system, affecting the overall device performance through the properties of the associated electrostatic double layer.[19]

Our study is devoted, in particular, to selected alkali carbonates such as Li_2CO_3, Na_2CO_3, K_2CO_3, whose melting temperatures range from $T_m = 996$ K in Li_2CO_3 to $T_m = 1164$ K in K_2CO_3. In applications, their liquid range can be extended downwards by considering mixtures of alkali ions. Binary mixtures of alkali-carbonates, in particular, typically exhibit at least an eutectic compositions whose melting temperature is below that of both pure components.[20] T_m can be further decreased by considering ternary[21] and higher mixtures, reaching its lowest known value at $T_m = 672$ K in the $Li_{0.90}Na_{0.62}K_{0.48}CO_3$ system.[21]

By molecular dynamics simulations we investigate structural and electrostatic properties of alkali carbonate / metal interfaces at relatively high temperature, of the order of $T \sim 1200$ K. The metal side of the interface is modelled at the atomistic but still very idealised level. The size of the atoms representing the metal electrode, as well as their geometrical arrangement, are intended to mimic the (111) surface of gold. Most of our simulations concerned neutral metal electrodes, but a few simulations for charged electrodes have been carried out as well. The ionic species on the liquid side are described by an empirical force field, based on rigid (i.e., unpolarisable) ions, whose parameters are taken from an early but still relevant model of alkali carbonates.[22,23]

From the theoretical and computational point of view, our simulations represent an important extension beyond the several computational studies of simple electrolytes made of spherical charged particles confined in between rigid structureless walls, which have been briefly reviewed in Ref. 24. Although a few studies of clean metal/molecular electrolyte interfaces have already appeared in the literature (see, for instance, Ref. 25,26), the simultaneous inclusion of the molecular nature of the electrolyte, and of the atomistic structure of the electrode is still a relative novelty.

Despite this inclusion of microscopic detail, our model interface is far from the complexity of solid electrolyte interfaces in rechargeable Li-atom or Li-air batteries[14], involving many other elements (graphite) and compounds (semi-carbonates), as well as exotic structures such as solid electrolyte interfaces.[27] The interest in high capacity batteries especially for automotive applications has driven a large number of computational and simulation studies of these interfaces, that, however, are markedly distinct from those we target in our study. Modelling of solid-electrode / molten carbonate interfaces in rechargeable batteries is a still rapidly developing field,[28] with ad-hoc force fields, often built on or complemented by ab-initio simulations.[29] In many cases, reactive force fields are strictly needed to describe the chemical equilibrium at these interfaces.[30]

Our simulations, instead, concern cleaner and simpler interfaces in electrochemical devices operating at relatively high temperature, based on pure alkali-carbonates and, more often, on their mixtures. As such, the model is expected to be relevant for MCFC, but also for the thermoelectric devices of Ref. 17.

Because of the simplicity of the model, the results of our simulations enjoy a broad relevance, highlighting features and properties arising from very general principles. Our results, in particular, provide an intriguing view of layering, ion-ion correlation parallel to the electrode plane, and screening of electrostatic perturbations at the interface, due to the interplay of charge and packing effects, and of broken symmetry at the metal/electrolyte boundary.

To establish a firm contact with previous studies, we carried out simulations for static and transport properties of homogeneous alkali carbonate liquid samples, whose results are briefly presented and discussed in the paper. Comparison is also made with the results of previous studies, devoted to simple, spherically symmetric particles confined by neutral or charged structureless planar walls.[24]

Experimental data are available to benchmark all simulation results, but they are not as detailed and as accurate as desirable, their quality being limited primarily by the challenge of dealing with high temperature samples made of corrosive compounds. Nevertheless, X-ray[32–34] and neutron diffraction[35] measurements, as well as Raman spectroscopy[31,32] have been carried out to characterise the structure and the vibrational dynamics of homogeneous (bulk) molten alkali carbonates and of their mixtures.

A few self-diffusion coefficients of molten alkali carbonates obtained by the tracer method are given in Ref. 36,37; more data covering a wider temperature range are obtained by light scattering, and in particular by the forced Rayleigh scattering method;[39] A critical assessment of the different measurements of diffusion coefficients in molten salts is given in Ref. 38. Thermal conductivity is reported by Nunes *et al.*[41], and by Egorov and Revyakin;[42]; fairly systematic data on electrical conductivity are listed in Janz and Lorenz.[43] The error bar on diffusion coefficients is of the order of $10 - 20$ %, and similar or larger relative error bars are estimated for the other transport coefficients.

One can easily observe that, in contrast to the surge of computational studies, most of the experimental measurements on bulk molten alkali carbonates are not very recent.

Experimental results on metal electrode / molten alkali carbonate interfaces are less systematic than for homogeneous liquid alkali carbonates, at least because the number of systems of interest increases rapidly when the composition, structure, electric and thermodynamic conditions of the electrode enter the picture. In fact, many voltammetry and a few vibrational (Raman, infrared) and optical spectroscopy (XPS, AES) measurements have been carried out, but seldom on clean and simple interfaces that could be considered as paradigmatic. The relevant experimental data will be reported and discussed in the results section when needed.

II. MODEL AND METHOD

A. Modelling approaches

The present state of metal carbonate models reflects the background and history of the computational communities interested in these systems. Early computational activity,[44–46] focused on lattice dynamics and using solid-state force fields,[1] concerned primarily carbonates of divalent metals, because of their role in mineralogy and geophysics.[6–9] Density functional computations for the structure, lattice dynamics and energetics of metal carbonate crystals[47,48] are relatively recent developments.

The interest in metal/carbonate interfaces[50,51] came next, motivated by the technological development and increasing application outlook of MCFC. The increasing role of alkali carbonates as MCFC electrolytes, often as eutectic mixtures, motivated density functional computations for surfaces of solid carbonates,[49] but never progressed to full blown molecular dynamics simulations of molten carbonate / solid metal interfaces. Because of computational cost considerations, the subject of homogeneous and inhomogeneous molten carbonates has been primarily the realm of empirical force fields.

Molten carbonates of geophysics interest, as well as MCFC interfaces, represent relatively simple and clean systems, and the two concerned communities developed and favoured comparatively simple model force fields, relying on non-polarisable ions, and rigid or flexible CO_3^{2-} ions described in atomistic detail. The simplicity of the model, in turn, endowed the force field with good transferability, and with a general reliability over a broad range of thermodynamic conditions. These positive features partly explain the long life span of these models in the otherwise rapidly evolving stage of force field modelling. Exemplary of this class of force fields are those developed by Janssen and Tissen,[22,23] and by Habasaki.[52] More recent examples of force fields developed according to the same strategy and to similar computational protocols are those of Ref. 53 and of Ref. 54.

Improvements on the basic models concerned primarily electric polarisation[55] and extension to cover other species such as water.[56,57] Including polarisation, in particular, appears to be required to achieve an accurate and reliable prediction of dynamical properties and transport coefficients. To some extent, the improvement in the description of these same properties can be achieved by tuning the intra-molecular force field for the carbonate ion, as done in Ref. 58, or by a more comprehensive re-parametrisation of the (still unpolarisable) force field, see Ref. 53.

More recently, the simulation activity on carbonates in lithium-atom and lithium air batteries surpassed, at least in volume, that for minerals and MCFC. In batteries, however, the electrolyte ions diffuse in a complex matrix, and the electrode/carbonate interface contains several additional components, reaching a complexity far higher than for metal/carbonate interfaces in fuel cells. Semi-carbonates and a host of neutral organic carbonate species play a role, and this complexity is reflected in the variety of models that have been developed, tuned and validated for specific systems and applications,[28,59] often combined with ab-initio approaches.[29]

Lacking extensive past modelling of metal / alkali carbonate interfaces, we cannot rely on the computational community expertise to guide our work for metal electrode / molten carbonate interfaces. The model we propose to describe these interfaces is described in the following subsection.

B. Force field definition

Since our interest is primarily focused on MCFC and in other relatively simple electrochemical interfaces, to model alkali-metal carbonates we resort to the force field of Janssen and Tissen (JT, Ref. 22,23), thoroughly tested and validated by a long sequence of previous studies, up to the very recent molecular dynamics simulations of Ref. 53,60

The JT model describes carbonates as assemblies of metal M^+ cations and CO_3^{2-} anions, where CO_3^{2-} consists of four interaction centres representing individual atoms of fixed relative geometry and D_{3h} symmetry, in which the oxygen atoms in CO_3^{2-} occupy the vertices of an equilateral triangle, whose centre of mass is occupied by the carbon atom.

The interaction among atoms on different ions is described through a Coulomb plus Born-Mayer-Huggins (BMH) short range potential:

$$V_{BMH}(r_{ij}) = \frac{z_i z_j e^2}{r_{ij}} + b\left(1 + \frac{z_i}{n_i} + \frac{z_j}{n_j}\right)\exp[\alpha(\sigma_i + \sigma_j - r_{ij})] \tag{1}$$

In this expression, r_{ij} is the distance between ions i and j, z_i is the valence of atom i whose charge is $Z_i e$, σ_i plays the role of an ionic radius and n_i is the number of electrons in the outer shell of atom i. The force field parameters have been set fitting the results of Hartree-Fock computations[22] for a single CO_3^{2-} ion and for the M_2CO_3 gas phase molecules. Partial charges on CO_3^{2-} are also selected on the basis of the Hartree-Fock results, while the charge of the M^+ cation is equal to the formal charge $+e$. These are crucial choices that, together with the neglect of polarisability, affect transport properties.[61]

The parameters from Ref. 22 are listed in Tab. I. The constant $b = 4.865$ kcal/mol determines the relative size of the Coulomb and short-range energy contributions, while $\alpha = 3.45$ Å^{-1} determines the steepness of the short range repulsive potential.

Following the original Janssen and Tissen prescription,[23] in our simulations the C−O bond length was constrained to 1.27 Å by use of the SHAKE algorithm[62]. The accuracy tolerance of the SHAKE solution was set to 10^{-7}, as suggested by Ottochian et al.[60], as they experienced energy drift with the use of looser tolerances.

By contrast, our description of bending and out-of-planarity deformations of CO_3^{2-} deviates from Ref. 22,23, since we experienced a loss of energy conservation upon imposing a fixed anion geometry by standard techniques to enforce constraints. To overcome this purely technical and rather minor difficulty, we introduced bending and out of planarity energy terms with ad-hoc force constants sufficiently large to ensure that discrepancies from the intended geometry are small. By comparison with published results from rigid-ion simulations we verified that this deviation from the standard scheme affects only slightly our results. The parameters defining this ad-hoc flexibility, not included in the original Jenssen and Tissen force field, are collected in Tab. II.

Since the force field does not include polarisability, and the CO_3^{2-} intra-molecular flexibility is only partially and empirically accounted for, we accept that the diffusion coefficient and electrical conductivity are underestimated, as already found in previous simulations using the same or a similar force field. This expectation is borne out by the simulation results reported in the following section.

The Hartree-Fock is generally viewed as an outdated approach, therefore we investigated the influence of higher level density functional approaches on the properties of ions and on the force field parametrisation. The results of this side issue are discussed in the Appendix.

While the alkali carbonate side of the interface is described at least semi-quantitatively, the metal side is admittedly more idealised. First of all, the metal electrode is represented by a single layer of Lennard-Jones particles arranged on a compact hexagonal geometry. To keep the mono-layer in place, the N_m metal atoms on the two metal electrodes are tethered by a harmonic spring to a geometric lattice $\{\mathbf{R_i}; i = 1, ..., N_m\}$ fixed in space and of the desired hexagonal geometry.

The potential energy of the metal layer, therefore, is:

$$U_m = \frac{4\epsilon_m}{2} \sum_{i \neq j}^{N_m} \left[\left(\frac{\sigma}{r_{ij}} \right)^{12} - \left(\frac{\sigma}{r_{ij}} \right)^{6} \right] + \frac{1}{2} k_{teth} \sum_{i}^{N_m} \mid \mathbf{R_i} - \mathbf{R_i^0} \mid^2 \tag{2}$$

Disregarding at first the particle-particle Lennard-Jones interaction, the potential energy for the metal layer represents a simple computational realisation of an Einstein model for a crystal with localised vibrations. In our simulations, the spring constant also reported in Tab. II is set to a value high enough ($k_{teth} = 50$ kcal mol$^{-1}\mathring{A}^{-2}$) to make sure that the metal surface is sufficiently rigid and 2D-dense to prevent ions from crossing the metal barrier. In principle, the spring constant could be tuned together with the Lennard-Jones parameters to reproduce the elastic properties of the underlying metal bulk.

Since efficient and reliable interatomic potentials for bulk metals and their surfaces are well known and widely used,[63,64] the choice of Eq. (1) for the metal potential energy is due exclusively to computational economy reasons.

The interaction of metal atoms with carbonate atomic species is given again by suitable Lennard-Jones interactions. The parameters for the atoms present in the carbonate liquid are taken from the OPLS model, and listed in Tab. III. These are combined with the metal

Lennard-Jones parameter using Berthelot'rule:

$$\sigma_{ij} = \frac{\sigma_{ii} + \sigma_{jj}}{2} \tag{3}$$

$$\epsilon_{ij} = \sqrt{\epsilon_{ii}\epsilon_{jj}} \tag{4}$$

In other terms, atoms belonging to the metal carbonate ions are described through the JT potential when interacting among themselves, and by the OPLS Lennar-Jones potential when interacting with the solid-like wall.

The most apparent limitation of the force field describe in this subsection is its neglect of image charge interactions at the metal electrolyte interface, that, again, can be seen as due to the absence of polarisability. We accept this limitation partly for the arguments of Ref. 65 suggesting that image charges are not very important for real interfaces, and, again, because of computer cost considerations. The GolP potential of Ref. 66 does cover image charges, but its implementation and usage in LAMMPS appear to be rather demanding for the long simulations required in our investigation. Moreover, the GolP assumption of fixed metal atomic positions is not justified at the high temperature of our simulations. Nevertheless, we adopt the Lennard-Jones diameter for particles used in GOLP, tuned on gold atoms. In some limited sense, therefore, our metal surfaces represent (111) surfaces of gold, although at the temperatures of our simulation gold is close to melting, its surface is reconstructed at least to the (1×23) form, and probably criss-crossed by a multitude of steps delimiting small compact terraces.

In our simulations all systems are modelled as periodic in 3D (details in Sec. III and in SI), and the Coulomb interactions are computed using Ewald summation (see, for instance, Ref. 67) in its particle-particle particle-mesh version.[68] Three-dimensional periodicity is assumed also for samples representing liquid slabs confined by solid metals electrodes. In this case, the periodicity along the direction perpendicular to the interface is only a formal device to allow us to use well known and widely implemented algorithms.[68] On the other hand, it affects the estimate of the electric field across the system. This effect will be taken into account and subtracted off, as explained in Sec. III B. Approaches to evaluate Coulomb interactions in systems periodic in 2D and in 1D are available,[69–71] but not implemented in popular MD packages, and experience in their performance and reliability is not extensive.

All simulations have been carried out using the LAMMPS package[72] on the supercomputers of the NOTUR centre. (to be completed)

III. RESULTS

The primary focus of our study are the interfaces between molten alkali carbonates and solid metal surfaces. Nevertheless, we also compute the properties of homogeneous liquid carbonates at equilibrium to validate our computational set up.

As already anticipated, all of our molecular dynamics simulations have been carried out using the LAMMPS package sampling different statistical mechanics ensembles, from NVE (microcanonical) to NVT and NPT. The integration time step is 1 fs in all cases.

A. Structure and transport coefficients of bulk Li, Na and K-carbonates melts

In the homogeneous case, samples consist of 512 M_2CO_3 molecules, with M being Li, Na or K.

Widely accepted approaches to enforce pressure and temperature are known to reproduce the correct distribution functions in a few ensembles of choice. Their effect on transport coefficients is somewhat less certain. To bypass any potential problem, we follow the protocol described in Ref. 60, used also in Ref. 53. For each sample, simulations are carried out at first for 100 ps in the isothermal-isobaric (NPT) ensemble using a Nosé-Hoover thermo- and barostat to prepare samples at pre-set values of temperature and pressure. The temperature was relaxed with a characteristic time scale of 0.1 ps, while the pressure was relaxed on a time span of 1 ps. After these first 100 ps, the barostat was discontinuously disconnected and the simulation continued for another 100 ps in the canonical (NVT) ensemble, keeping the sample close to the target temperature.

Finally, a 5 ns production run was carried out in the microcanonical (NVE) ensemble. From this run, temperature, pressure and energy were stored every 0.1 ps. Atomic coordinates and velocities were stored with the same 0.1 ps periodicity on a trajectory file for further analysis. Note that neither the pressure nor the temperature are exactly imposed through this protocol, which only aims at approaching the target (T, P) by applying the least perturbation to the system.

Following again Ref. 60, simulations were carried out at a pressure close to 15 kbar, to compensate for the slight under-estimate of the equilibrium density by the JT potential. Ref. 53 adopted the alternative strategy of tuning a force field to obtain a better estimate of the equilibrium density, at the cost of loosing a direct comparison with previous studies using the JT potential.

The target temperatures of our simulation have been $T = 1200$ K, 1300 K, 1400 K and 1500 K. These high values have been selected to make sure that the system is in the equilibrium liquid phase, despite the relatively high melting temperature of real (pure) alkali carbonates, the uncertainty on the unknown melting temperature of model carbonates, and despite the 15 kbar pressure applied during the simulation.

In reality, thermal decomposition of alkali carbonates starts right above the melting temperature, even though in most cases it proceeds fairly slowly up to their boiling point (see, for instance, the experimental analysis of the thermal decomposition of Na_2CO_3 in Ref. 73).

In the production stage of our simulations, only the system volume is directly assigned in input, while the average temperature and pressure of the run are computed a posteriori from the trajectory. For this reason, we list the nominal and actual temperature and pressure of each run in Tab. IV. The equilibrium volume, determined in the (NPT) stage of sample preparation, is also listed in Tab. IV, and it is the first quantitative property we discuss. A quick look into standard tables of ionic radii ($R_{Li^+} = 0.90$ Å , $R_{Na^+} = 1.16$ Å , $R_{K^+} = 1.52$ Å, $R_{CO_3^{2-}} = 1.78$ Å , from Ref. 96) shows that the equilibrium volume exceeds the sum of the ions' volume by more than a factor of two, because of interstitial spaces, some of which are relatively large and empty. To partition space into contributions for cations and anions, we resort to an analysis of Voronoi polyhedra. To overcome the difficulty of large samples and disordered configurations, we resorted to a statistical Voronoi construction briefly described in the SI, and that might be seen as an application of Monte Carlo integration. The results are shown in Tab. V. We verified that the relative change of cation volume in going from Li_2CO_3 to Na_2CO_3 and K_2CO_3 is significantly less than the corresponding change of the ions' volume estimated on standard values of the ionic radius. Moreover, also the volume assigned to the anion increases slowly along the same sequence, causing only a modest decrease of the anion volume fraction from Li_2CO_3 to K_2CBO_3.

1. *Structural properties*

Plots of the radial distribution functions at $T = 1200$ K and $P = 15$ kbar for C-C, C-M, O-M and M-M pairs in M_2CO_3 can be seen in Fig. 2.

As expected, our results agree with those by Tissen and Janssen.[22,23] They also agree with those of previous studies base on rigid ion models.[52,53,60,74] Moreover, the partial radial distribution functions display features characteristic of ionic systems. First of all, the sum of the ionic radii listed in the previous sub-section is a fair predictor of the position of the cation-anion radial distribution function over the entire temperature range. We observe, in particular, that the main peak of g_{Li-O} is higher and closer to the origin than the main peak of either g_{Li-Li} and g_{O-O}, reflecting the fact that the attractive cation-anion Coulomb interaction is certainly not the average of the cation-cation and anion-anion interactions, thus violating the simple additive (Berthelot's) picture. Moreover, we observe the regular alternation of positive and negative charge oscillations that, again, characterise the radial distribution of ions in molten salts. In general, the radial distribution functions of alkali carbonates are closer to those of simple ionic system than to those of molecular systems, emphasizing again the relative simplicity of the CO_3^{2-} anion.

We comment here also on the oxygen-oxygen radial distribution function $g_{OO}(r)$, reported in Fig. XXn of the Supplemental Information. In all cases, the $g_{OO}(r)$ function displays a high and narrow peak at $r = 2.2$ Å accounting for intra-CO_3^{2-} correlations. As expected, this peak hardly changes with M_2CO_3 compound and simulation temperature. Inter-CO_3^{2-} correlations are described by broad peaks in $g_{OO}(r)$ for $r > 2.5$ Å . For each M_2CO_3, the temperature dependence of $g_{OO}(r)$ is mild. On the other hand, $g_{OO}(r)$ changes in a characteristic way along the Li_2CO_3, Na_2CO_3, K_2CO_3 sequence. In going from Li_2CO_3 to Na_2CO_3, for instance, this change consists primarily of a linear scaling of the radial distance, reflecting the general expansion of the system volume, and conserving the characteristic double-hump shape of the second peak in g_{OO}. The result for K_2CO_3 is somewhat different, since the broadening of all peaks causes the partial loss of the double hump. The change, however, does not seem so drastic to point to a basic change in the local arrangement among oxygen atoms. Similar observations apply to the oxygen-carbon and carbon-carbon distributions (not shown). Hence, we can think of the CO_3^{2-} distribution as fairly similar for the three compounds, providing the neutralising background for the distribution of cations into the system.

To better characterise the local arrangement of atoms into the liquid, the coordination number of the first shell was found by integrating the partial radial distribution functions according to:

$$N_{ij} = \frac{N_j}{V} \int_0^{R_{ij}^{min}} g_{ij}(r) 4\pi r^2 dr \tag{5}$$

where R_{ij}^{min} is the minimum of the corresponding radial distribution function $g_{ij}(r)$ following its first peak. The results are collected in Table VI. By symmetry of the g_{ij}, the coordination of atom type i by type j atoms (N_{ij}) is N_j/N_i times the coordination of atom type j by type i atoms (N_{ji}).

The local arrangement of metal cations is easily rationalised starting from the configuration of the oxygen atoms, that represent the space filling element. At the high temperature of our simulations, the signature of the first oxygen-oxygen coordination shell is not very strong, but the corresponding coordination number computed according to Eq. 5 is invariably very close to 12, pointing to a compact packing of oxygen atoms. Needless to say, the structure cannot be any ideal fcc, hcp, etc., since each oxygen has two very close neighbours belonging to the same carbonate unit.

It is well known that the packing of spheres leaves tetrahedral and octahedral interstitial sites, which cations occupy according to their size and charge.[85] Tetrahedral sites, in particular, are the smallest void, and we find that, indeed, the coordination number of Li^+ by oxygen in Li_2CO_3 is four, confirming that the small Li^+ ion occupies a tetrahedral interstitial site in the oxygen structure. Because of the larger size of the K^+ ion, in K_2CO_3 we find a cage of six oxygen atoms around the metal ion, suggesting that it occupies an octahedral site. The same coordination numbers in Li_2CO_3 and K_2CO_3 were also found from simulation by Koishi et al.[74].

The coordination number of Na^+ by oxygen in Na_2CO_3 appears to be five, which agrees with the value from Wilding et al.[58] obtained from simulation at $T = 1750$ K. No simple geometry has five-fold coordination, which appears to be the average of four-fold and six-fold coordinated metal sites. Apparently the Na^+ radius is close to the transition between being stable in the tetrahedral and in the octahedral sites, hence this cation is statistically distributed among all the interstitial sites.

As can be seen from Table VI, the coordination number changes very little with temperature in the range $1200 \leq T \leq 1500$ K. This means that raising temperature from $T = 1200$ K up to $T = 1500$ K does not change the cations' preference for the tetrahedral or octahedral interstitial site, that depends primarily on the cation size.

Early X-ray diffraction data from Ref. 34 are fully compatible with the increase of cation coordination by oxygen in going from Li_2CO_3 to K_2CO_3.

The number of CO_3^{2-} ions around each cation is apparently given by the cation coordination by C atoms, that turns out to be close to 4 irrespective of temperature and only slightly dependent on the cation chemical identity. The coordination number for carbon increases a bit in going from Li_2CO_3, Na_2CO_3 and K_2CO_3, but this increase is less than the increase in the cation coordination number by oxygen. This would mean that nearly the same number of carbonate ions surround each cation. To account for the change in the M-oxygen coordination, we need to conclude that for the heavier cations the carbonate ions are oriented so that more oxygens are within the first coordination shell. This can be explained as the heavier cations are larger, giving more surface area and therefore more space for the oxygens around them.

To summarise these observation, one could state that the usual description and trends discussed long ago for solid silicates[85] remain approximately valid in the case of molten alkali carbonates, despite the obvious distortions imposed by the molecular structure of the cation.

2. *Structure factor*

To be able to compare with experiments, we calculated the partial structure factors $S_{ij}(k)$ as a function of wave number k. The complete description of scattering, requires to consider $S_{ij}(k)$ for all the $\{i, j\}$ pairs corresponding to the metal, carbon and oxygen atoms in the system. Instead, we adopt a simplified description based on a two component (cations and anions) picture, obtained by identifying the anion position with the carbon atom in CO_3^{2-}. Moreover, to ease the interpretation of the results, we combine the $S_{++}(k)$, $S_{+-}(k)$ and $S_{--}(k)$ into a number(NN) and a charge (QQ) structure factor,[75] defined as:

$$S_{NN}(k) = \frac{1}{2}\left[S_{++}(k) + 2S_{+-}(k) + S_{--}(k)\right] \tag{6}$$

$$S_{QQ}(k) = \frac{1}{2}\left[S_{++}(k) - 2S_{+-}(k) + S_{--}(k)\right] \tag{7}$$

where the fact that anions and cations have the formal charge $\pm e$ has been implicitly take into account. The third function $S_{NQ}(k)$ nearly vanishes for all k, and for this reason is not reported or discussed below.

The result for Li_2CO_3 and Na_2CO_3 can be seen in Figure 3.

Several observations are worth noting. First of all,[75] the $k \longrightarrow 0$ limit of the number-number structure factor is proportional to the value of the isothermal compressibility χ_T, divided by the ideal compressibility at the same density and temperature:

$$\lim_{k \to 0} S_{NN}(k) = \rho k_B T \chi_T \tag{8}$$

In this equation, k_B is Boltzmann's constant and ρ is the number density. As expected, the compressibility is relatively low, because of the high density and strong correlations among ions.

The shoulder at $k \sim 1.8$ Å^{-1} apparent in the lithium S_{NN} and absent in the Na_2CO_3 case is an important feature, pointing to a supramolecular clustering of the ions in Li_2CO_3 (but not in Na_2CO_3), possibly due to the small size and strong polarising potential of the Li^+ ion. It could be due, for instance, to some residual regularity in the geometrical disposition of the tetrahedra occupied by Li^+ in the oxygen structure. Unfortunately, such regularity cannot be easily recognised in the disordered structure of the liquid phase.

Comparison with neutron scattering data is affected by the large uncertainty of the experimental measures, and by the difficulty of disentangling the contributions of different atom pairs from a single scattered intensity, since isotopic substitution is nearly ineffective in carbonates). As a result, it is difficult to assess the origin of the agreement or disagreement between simulation and experiment, although the two sets of data are certainly in relatively close correspondence. For instance, if one is to compare with the literature, e.g. the neutron scattering experiments by Kohara et al.[35], one would find the highest peak for Li_2CO_3 at 1013 K to be ~ 3 and located around $k = 2.5$ Å^{-1}, while in our case the peak is below 2 but still located around $k = 2.5$ Å^{-1}. In this case, the difference in the peak hight might also be due to the different temperatures of the computational and experimental samples. For completeness, we report that Ohata et al.[76] calculates the structure factors from density functional theory (DFT) computation for a Li_2CO_3 tetramer. The values from this paper are very similar to the ones by Kohara et al.[35] However, calculating the structure factor from the periodic replication of as little as four molecules is not very accurate, so this result is to be taken with some skepticism.

Comparison with X-ray scattering data is even more challenging than in the case of neutrons, since the experimental signal has to be deconvoluted from the form factors for atoms and ions which are known only from approximate electronic structure computations. Nevertheless, the recent high energy X-ray diffraction data from Ref. 58 represent an obvious term of comparison for simulation. To avoid the complication of the atomic form factors, we did not compare the partial structure factors directly, but we compared the radial distribution functions from our simulation with those reported in Ref. 58. The height and position of peaks and valleys of the partial radial distribution functions agree for the two sets of data, despite some slight quantitative differences along the g_{ij} functions. Since in Ref. 58 the total structure factor from simulation and from X-ray diffraction do agree, by the transitive property we conclude that also our structure factors agree with X-ray diffraction, at least in the combined form of a total structure factor. However, more systematic comparisons are in order since they provide an unambiguous assessment of the quality of the force fields used in simulations.

The charge-charge structure factor $S_{ZZ}(k)$ as a function of k has also been computed, and can be seen in Figure 4.

Comparing this figure to Figure 3, one can observe that the peak for S_{ZZ} is higher than for S_{NN}, pointing to Coulomb correlations being stronger that ion packing effects, as seen also in the structure factor of simple molten salts.[75]

Mixtures of molten alkali carbonates play a preferential role in applications, because their melting temperature can be lower than that of either pure components. We carried out a limited exploration of an equimolar Li and Na carbonate mixture at $T = 1300$ K. Samples contained 512 $LiNaCO_3$ molecules, and simulations lasted 5 ns after an equilibration stage of 1.4 ns.

We focus here on the structure factor, that we computed to gain insight on the miscibility between the two pure components, or, more precisely, to reveal signs of a miscibility gap. To this aim, we consider the system as made of two positively charged components, consisting of Li^+ and Na^+, while the carbonate anions are treated as a structureless continuum of negative charge, needed to ensure the system neutrality. We compute both the number-

number structure factor:

$$S_{NN}(k) = \frac{1}{2}\left[S_{LiLi}(k) + 2S_{LiNa}(k) + S_{NaNa}(k)\right] \tag{9}$$

as well as the concentration-concentration structure factor, defined as:

$$S_{cc}(k) = \frac{1}{2}\left[S_{LiLi}(k) - 2S_{LiNa}(k) + S_{NaNa}(k)\right] \tag{10}$$

Our interest in $S_{cc}(k)$ is due to the fact that:

$$\lim_{k\to 0} S_{cc}(k) = \rho k_B T \chi_c \tag{11}$$

where χ_c is the static concentration susceptibility, which grows (in fact it diverges) at the opening of a miscibility gap.

The results of our simulations are shown in Fig. 5. The low value of $\lim_{q\to 0} S_{NN}(q)$ points to the virtual incompressibility of the cations' fluid. The concentration-concentration structure factor, instead, is nearly constant at $S_{cc}(q) \sim 1$. Strictly speaking, this result rules out a miscibility gap, but it also shows that large concentration fluctuations of long wavelength are likely, and opposed only by low resorting forces, implying, in turn, slow relaxation of any concentration imbalance. These considerations will become relevant in the interpretation of the results for inhomogeneous $LiNaCO_3$ mixtures confined by solid-like walls presented in Subsect. III B

3. Transport properties

The mean square displacement for Li^+ and CO_3^- in Li_2CO_3 at $T = 1200$ K and $P = 15$ kbar is shown in Figure 6, for up to 1 ns. The quantity reported in the plot is defined as:

$$MSD_\alpha(t) = \frac{1}{N_\alpha}\sum_i \langle |\mathbf{r}_i(t+t_0) - \mathbf{r}_i(t_0)|^2 \rangle_{t_0} \tag{12}$$

where $\mathbf{r}_i$ is the coordinate of an atom of species α, and N_α is the number of atoms of that same species. The average over the reference time t_0 spans the entire $5 - t$ ns available from the simulation trajectory.

As can be seen, the MSD is quite linear for both the cation and anion, confirming that the system is in the liquid state. Also in this case, *cations* are identified with the carbon atom at the centre of CO_3^{2-}. The results shown in this plot are representative also of those obtained for the other carbonates we investigated.

Tab. VII, Tab. VIII and Tab. IX show the computed transport properties for Li_2CO_3, Na_2CO_3 and K_2CO_3, respectively.

The diffusion coefficient, computed by the Einstein relation:

$$D_\alpha = \lim_{t\to\infty} \frac{1}{6t} MSD_\alpha(t) \tag{13}$$

agrees well with previous simulations of alkali carbonates at comparable conditions and using a similar force field.[53,60]

An Arrhenius-like exponential fit allows us to compute activation energies for diffusion, reported in Tab. **??** for both ions. The fit, in turn, can be used to interpolate our data, or moderately extrapolate them outside the temperature range covered by simulation. Since the diffusion coefficients computed by our simulations agree with those of similar studies, also the activation energies tend to agree fairly well among different simulations, with, however, a few systematic quantitative differences. The activation barriers for cation and anion diffusion computed in our simulations, for instance, tend to be slightly higher than those of Ref. 60, and somewhat lower than those of Ref. 53. In general, the activation barrier for diffusion is remarkably low for a material whose applications concern temperatures approaching and sometimes exceeding $T = 1000$ K.

The good agreement, unfortunately, does not extend to the experimental results, as already noted in Sect. II. It is apparent that the computed diffusion coefficients tend to be less than their experimental counterparts, and the activation barriers are underestimated (check!) by the JT model. The statement generally applies both to cations' and to anions' diffusion, and the authors of previous studies argued that the discrepancy is due to the neglect of polarisability by rigid ion force fields. While we find this argument to be relevant, we also remark that the relative error bar on the experimental data[38] is between 10 % and 20 %, and the underestimation of self-diffusion by simulation is not without exceptions, see the overestimation of K^+ mobility at low temperature in the simulations of Ref. 53. Moreover, the comparison of experiments and simulations is often indirect, since the corresponding data refer to different temperatures, and the comparison relies on the Arrhenius fit introduced in the previous paragraph.

The authors of Ref. 58 point out that stiffening the intramolecular bonds in CO_3^{2-} results in a systematically smaller diffusion coefficient for the sodium ion, perhaps suggesting that the rigidity of the CO_3^{2-} unit in the JT force field might be responsible for its underestimation of the Na^+ diffusion constant. While this argument is likely to be at least partly true, the ab-initio computations described in the Appendix suggest that the CO_3^{2-} ion is too small and too rigid to deform significantly even at temperatures in excess of 1000 K, and the effect of CO_3^{2-} deformation on diffusion is not likely to be large.

At the very least, however, all classical simulations confirm the experimental finding that the ionic mobility is due primarily to cations,[86] contrary to early speculations attributing a special role to anions in self-diffusion.[87]

The electric conductivity computed by the Green-Kubo route:

$$\kappa = \frac{V}{3k_BT}\int_0^\infty \langle \mathbf{J}_Q(t)\mathbf{J}_Q(0)\rangle dt \tag{14}$$

is shown in Tab. ??. We verified that these results agree with those from the Einstein route, expressed by the relation:

$$\kappa = \frac{1}{K_BTV}\lim_{t\to\infty}\frac{1}{6t}\left\langle\left|\sum_i q_i[\mathbf{r}_i(t)-\mathbf{r}_i(0)]\right|^2\right\rangle \tag{15}$$

The underestimation of self-diffusion by our model force field is reflected in a similar underestimation of electrical conductivity, apparent from the comparison of computed and measured results.

In particular, from Janz and Lorenz[43], the electrical conductivity at $T = 1118$ K is $\kappa = 4.959$ S/cm. This is the highest temperature at which they measured conductivity for for Li_2CO_3. Since κ has a positive correlation with respect to temperature, both in my simulations and in the measurements by Janz and Lorenz, κ at $T \approx 1200$ K should be higher than the value Janz and Lorenz found at $T = 1118$ K. Ottochian *et al.*, which also uses the force field by JT[22], uses a scaling factor of ~ 1.7 on the electrical conductivity to better reproduce the experimental values. The authors of this paper argue that such a scaling factor could mimic the effect of using classical simulation instead of quantum mechanics, underlying the dynamics of experimental systems. This argument, however, is not fully developed and quantified. However, the success of this multiplicative adjustment has the merit of showing that the discrepancy between simulation and experiment concerns the pre-factor of the Arrhenius fit to conductivity more than its exponential parameter representing the activation energy for electrical conductivity.

A simple approximation to estimate conductivity is expressed by the Nernst-Einstein relation, based on the assumption that ions diffusion is uncorrelated:

$$\kappa_{NE} = \frac{F^2}{RT}\frac{\rho}{M_w}\left(\nu_+ z_+^2 D_+ + \nu_- z_-^2 D_-\right) \tag{16}$$

Ion-ion correlation, however, is always present, and almost without exceptions comparison of the NE prediction with experimental or simulation data for the electric conductivity of ionic fluids shows systematic differences. This observation lead to a modification of the NE equation into:

$$\kappa'_{NE} = \kappa_{NE}\left(1 - \Delta\right) \tag{17}$$

The Δ parameter is attributed to cation-anion pairing, resulting into flow without net electric current. Hence, pairing decreases conductivity, and Δ is expected to be positive. For alkali halides, for instance, Δ is ~ 0.26[60]. It is worth noting that the electrical conductivity we estimated by the Nernst-Einstein equation, eq. (16), is lower than the one computed with the Green-Kubo relation, eq. (14), for all systems at all temperatures. In order to get the GK values by the modified Nernst-Einstein relation, Eq. (17), Δ would have to be around -0.2.

This result does not violate any known constraint, and in fact negative Δ values have been repeatedly obtained in simulations (see, for instance, 79–82). The explanation could be due to "opposition of phase" correlation in the motion of the cations and anions, similar to back-flow in many-electron systems.[83] This effect could also be described saying that, in dense fluids, the motion of one ion in the positive direction pushes counter-ions in the opposite direction, enhancing electrical conductivity.

Still, if one is to calculate Δ from the experimental data for Na_2CO_3 (taking the values for diffusion coefficient by Spedding and Mills[77] and the density and electrical conductivity by Janz and Lorenz[43]), one would find that $\Delta \sim 0.3$. Thus, simulation and experiment apparently differ in this essential aspect, perhaps, once again, because of the neglect of polarisability in the simulation model. Nevertheless, it is certainly true that in the simulated model ion-ion correlation enhances electrical conductivity with respect to the ideal NE value.

The electrical conductivity can be seen to decrease as the cation goes down the period of the alkali metals. This can also be seen in the measurements by Janz and Lorenz[43], and, in principle, it might simply reflect the slowing down of dynamics with increasing mass of the diffusing species. It would be interesting to investigate whether the change from tetrahedral to octahedral coordination also plays a role. Our simulations, however, are not sufficient to this aim.

Last but not least, we conclude our analysis of transport coefficient by discussing thermal conductivity, computed by a Green-Kubo approach. The results of our simulations are reported again in Tab. VII, Tab. VIII and Tab. IX.

The literature values for the thermal conductivity λ are scarce and with large errors, due to the difficulty of measuring this property accurately at temperatures exceeding 10^3 K, as discussed by Nunes *et al.*[41]. This makes simulation particularly useful. Gillis et al.[40] presents the thermal conductivity of molten Li_2CO_3 measured using forced Rayleigh scattering with a CO_2 laser. In the temperature region $1070-1355$ K, λ is more or less constant ≈ 1 W m^{-1} K^{-1}. However, the accuracy of these measurements are $\sim$ 20%. If there is a temperature dependence, it is smaller than this error bar. The lack of temperature dependence can also be seen in the results of our simulations, but the computed values are larger than the experimental ones by a factor $\sim$ 3-4. We do not have an explanation of this large difference, apart from the fact that, as for most anharmonic properties, conductivity is not included among the properties that determine the force field through the initial fit of data computed for low energy configurations.

Numes et al. estimate that at 1173 K, $\lambda = 0.822$ W m^{-1} K^{-1} for Na_2CO_3, but discuss that the difference between different authors can be as large as 50%. Therefore, the values obtained by simulation for the thermal conductivity might very well be correct for Na_2CO_3.

Moreover, in Ref. 40 the work by Egorov and Revyakin is presented, where the steady state concentric cylinder method was used to find the thermal conductivity for molten Li_2CO_3. Here, $\lambda \approx 2$ W m^{-1} K^{-1} at 1000 K and $\lambda \approx 3$ W m^{-1} K^{-1} at 1300 K. However, Gills et al. believes that the Rayleigh scattering technique is superior when it comes to measurement of thermal diffusivity of high temperature molten salts, so the values from that method can be believed to be most accurate.

Although a quantitative agreement of computed and experimentally measured thermal conductivities is still far away, it is apparent that both simulations and experiments agree in attributing a remarkably large thermal conductivity to molten alkali carbonates, consistently with their role of heat transducers in many applications.

Thermal conductivity for pure molten K_2CO_3 is, as of this time, lacking. However, Zhang and Fujii[78] reports thermal conductivity for a 70/30 mol% mixture of molten Li_2CO_3−K_2CO_3. At $T = 922$ K, $\lambda = 0.829$ W m^{-1}K^{-1}. Therefore, it is reasonable to expect that the values obtained by simulation for the thermal conductivity of pure molten K_2CO_3 are of the correct order of magnitude.

B. Inhomogeneous system

Most of our simulations for the inhomogeneous system were done using 2048 M_2CO_3 molecules enclosed into an orthorhombic cell, limited along the z direction by two layers of atoms arranged on an hexagonal lattice (see Sec. II) along the xy plane. The cell is periodically repeated in x and y to represent a carbonate slab confined between two planar, parallel metal electrode surfaces at separation d_z. The value of d_z was chosen in such a way that the pressure on the particles confined between the walls would be close to the pressure in the homogeneous case. The force constant K_{thet} of the springs used to tether the wall atoms to the underlying hexagonal lattice was set to $K_{teth} = 50$ kcal mol^{-1} Å $^{-2}$.

The relatively large number of molecules in the simulation is imposed by the need to have a locally homogeneous fluid phase far enough from the wall, so that a clear distinction between the interface and the bulk can be made.

For reasons of computational convenience, the entire slab is periodically repeated also along z with a period L_z somewhat larger than d_z, leaving a gap between successive replicas of the slab. A drawing of the simulation geometry, illustrating the position and width of the gap, is shown in Fig. [...] of the SI. The aim of the gap is to decouple fluctuations at interfaces otherwise contiguous because of periodic boundary conditions. Hence, a wide gap is desirable, but computationally expensive: because of the reciprocal space term in the Ewald sum, the cost of computing the Coulomb energy of a fixed number of atoms increases linearly with the system volume. In our simulations, we set $L_z = dz + 8$ Å as a trade-off between saving on the empty space and having a distance between the walls sufficient to prevent sizeable spurious correlations. Test computations described in the Supporting Information allowed us to verify the adequacy of this choice for neutral interfaces. Computations with a net surface charge on the metal side of the interface require some additional care, as described below.

For all samples and temperatures, the molten carbonate / metal interface has a 36.047 ×

36.7038 Å^2 cross area, determined by the number, size and geometric arrangement of the tethered particles representing the confining wall. To account for the different molecular volumes, the periodicity of the simulation box along z has been set to $L_z = 150$ Å for Li_2CO_3, $L_z = 169.5$ for Na_2CO_3, $L_z = 226$ Å for K_2CO_3, and $L_z = 161$ Å for the single simulation of $LiNaCO_3$ in a confined slab. The choice of L_z does not determine the thermodynamic width of the molten carbonate slab, that we compute as follows. First, we compute the average number $\langle N_+ \rangle$ of cations and $\langle N_- \rangle$ of anions in a relatively wide region at the centre of the liquid slab, covering ~ 25 % of its width, and representing our identification of the bulk liquid phase. In Li_2CO_3, for instance, the width W_{bulk} of this bulk-like region was set to $W_{bulk} = 40$ Å , while we used $W_{bulk} = 48$ Å and $W_{bulk} = 60$ Å for Na_2CO_3 and K_2CO_3, respectively. After very minor corrections to $\langle N_+ \rangle$ and $\langle N_- \rangle$ to enforce charge neutrality, the bulk density of molecules is computed as:

$$\rho_b^{mol} = \frac{\langle N_- \rangle}{S_c W_{bulk}} = \frac{\langle N_+ \rangle / 2}{S_c W_{bulk}} \tag{18}$$

where S_c is the simulation box cros-section. Then, the width W_l of the liquid slab is computed as:

$$W_l = \frac{N_{mol}}{S_c \rho_b^{(m)}} = \frac{N_{mol} W_{bulk}}{\langle N_- \rangle} \tag{19}$$

where N_{mol} is the number of M_2CO_3 molecules in the system. The results are reported in Tab. X.

Shorter simulations were also done for Li_2CO_3 at $T = 1300$ K in which the system size were doubled and quadrupled along the y-direction, up to a maximum cross section of 36.047×146.82 Å^2. The first aim of these larger simulations was to quantify finite size effects on the results. More importantly, the large interface areas allowed us to get a peek at long range correlations along the surface.[84]

In what follows, we will assume that the $z = 0$ plane represents the middle of the simulation cell, and of the molten carbonate layer, that, therefore, extend over $[-\frac{L_z}{2}; \frac{L_z}{2}]$ and $[-\frac{W_l}{2}; \frac{W_l}{2}]$, respectively.

Before describing the electrostatic double layer on the electrolyte side, let us comment on the geometry of the metal side of the interface. In statistical mechanics, a surface is *rough* if the height-height correlation function diverges logarithmically with increasing distance along the surface. In our samples, metal particles are tethered by a harmonic spring to a geometric plane, and it is easy to show that the surface is statistically smooth by construction. Nevertheless, at $T \geq 1200$ K, the surface is locally disordered (see Fig. 7), thus mimicking the highly stepped appearance of gold surfaces at high temperature.[92]

The simulation was done with a time step of 1 fs in the NVT-ensemble enforces by a Nosé-Hoover thermostat. The relaxation time for the temperature was the same as in the homogeneous case, i.e. 100 fs. For each system, we carried out from 10 to 14 runs, each consisting of 10^5 steps, resulting in up to 1.4×10^6 steps in total (1.4 ns). A few of these runs were needed for equilibration. When the main quantities monitored during our simulation appeared to settle at a stationary value, we considered equilibration to have been achieved, and the rest of the runs represented our statistics stage. In Figure 8, the density profile for anions, cations and neutral particles can be seen for Li_2CO_3 at 1300 K.

The goals of the simulations is to investigate layering of the carbonate ions next to the metal surface, and to characterise the properties of the electrostatic double layer (EDL), which, even in the absence of a net charge distribution on the metal surface, forms because of the asymmetry between the ions, and from their unequal interactions with the metal atoms. A visual impression of these effects is given in Fig. 9, showing the charge density profile across the interface between Li_2CO_3 and the model electrodes. A prominent peak is apparent in both profiles at contact, followed by a fairly extended sequence of oscillations of decreasing amplitude and constant wavelength. The decay length and oscillation wavelength are nearly the same for the mass and charge density profiles, while the phases differ by $\sim \pi/2$ rad. Slight anomalies are apparent at near contact, where the liquid phase has to match the solid-like wall.

The density profile next to the metal surface is largely determined by requirements of constant pressure across the interface, as stated by several contact theorems,[24] strictly valid, however, only for somewhat idealised systems. The quantitative details of the mass density profile, therefore, depend directly on the pressure and temperature of the system.

The charge density profile, on the other hand, reflects perfect screening conditions,[88] imposing the exponential decay of every charge perturbation in an equilibrium fluid system containing charged particles. At variance from the (monotonic) exponential decay predicted by simple theories such as Poisson-Boltzmann[90] and Debye-Hückel,[91] screening is short range but oscillating at the density and temperature conditions of our simulations.

Because of the diffuse character of the ion profiles, the absorption of ions at the interface does not need to vanish, provided the charge of absorbed cations and anions is the same. Then, if we define:

$$\Gamma = \int_{-L_z}^{-W_l} \left[\rho_{CO3}(z) - \rho_b^{mol}\right] dz = -\int_{-W_l}^{0} \left[\rho_i(z) - \rho_b^{mol}\right] dz = \tag{20}$$

$$\int_{-L_z}^{-W_l} \left[\rho_{M^+}(z) - 2\rho_b^{mol}\right] dz = -\int_{-W_l}^{0} \left[\rho_{M^+}(z) - 2\rho_b^{mol}\right] dz$$

we obtain the results in Tab.XX (data available). Because of the repulsive solid-like wall, Γ is small, but still represents a crucial parameter for the thermodynamic description of the interface.

As already stated, oscillations continue well into the fluid phase. Fig. 9 shows that, as expected, the amplitude of the oscillations decreases with increasing temperature, while their phase is almost unaffected. A similar effect is observed upon decreasing the pressure, as shown in Fig. 13, comparing the charge density profile for Li_2CO_3 at $T = 1300$ K at $P = 7$ kbar and at $P = 11$ kbar. We point out that the simulations of the inhomogeneous systems could not be done at exactly the same pressure of the corresponding homogeneous samples, but at pressures shown in Table XII. This is due to the inaccessibility of the NPT ensemble in our simulations, since the molten carbonate slab is confined by the wall fixed to anchor points whose position is fixed at the beginning of the simulation.

A detailed analysis of the simulation trajectories reveals a wealth of microscopic information on these systems. In all of our samples, cations are at least somewhat smaller than anions, hence we observe that cations reach closer to the wall than anions. Moreover, cations represent the majority of the ions in the first peak closest to the neutral wall. This numerical predominance, however, is mainly a consequence of stoichiometry. Once the density profiles along z are normalised to the bulk density of each species, the highest peak at the interface belongs to CO_3^{2-}, hence the largest amplitude peak in the charge density profile corresponds to negative charge (see the arrows in Fig. 9). Most of these features depend on the asymmetry in the ion size, become less apparent in going from Li_2CO_3 to Na_2CO_3, and almost disappear in K_2CO_3.

Inspection of simulation snapshots reveal that in all cases the CO_3^{2-} anions orient themselves parallel to the metal surface, and form an approximately hexagonal lattice (see Fig. 10). The structure of lithium ions (not shown in Fig. 10) in the contact layer locally displays clear motifs of hexagonal symmetry, but ordering is blurred already on the nm scale by a multitude of defects.

Because of the great role of contact theorems, expressing the mechanical stability of interfaces, these results are expected to be sensitive to the bulk density and temperature through the bulk equilibrium pressure.

We now discuss the effect of the interface on dynamical properties, using diffusion as a paradigmatic case. A fully quantitative discussion is not easy, since particles move freely in and out of any finite layer at the interface. Moreover, the centre of mass of this variable set of interfacial particles is not fixed, thus blurring the definition of the self-diffusion coefficient. To provide a semi-quantitative characterisation of diffusion at the interface, we adopted the following operational definition. First, at a given time t_0, we identify all the ions belonging to the density layer (3 Å width) in contact with the wall of neutral particles. Then, we computed the mean square displacement of only these labelled cations and anions as a function of time for $(t - t_0)$ up to 50 ps, and we averaged over t_0, using the long trajectories generated during the simulation.

The results of this lengthy analysis can be qualitatively summarised as follows. As expected, in proximity of the interface diffusion is apparently anisotropic, being slower in the z direction than along x or y. Apparently, the density layering along z effects diffusion more than the corrugation of the solid-like surface along xy. Moreover, even the relatively fast diffusion along xy at the interface is still slower than diffusion in the bulk. A simple scaling factor has been included to account for the different dimensionality of diffusion in the xy plane and in the bulk. The simplest explanation for the in-plane slowing down of diffusion involves the corrugation of the interfacial region due to the atomistic representation of the solid-like surface. Slowing down of diffusion could also be due to the overcrowding of ions at the interface.

The relative size of all these effects depends on the choice of the M metal in $\mathrm{M_2CO_3}$. Simulation temperature and pressure play a complementary role. Effects due to the proximity of the solid-like wall are apparently and systematically more important for $\mathrm{CO_3^{2-}}$ than for cations. They are also more apparent for $\mathrm{Li_2CO_3}$ than for either $\mathrm{Na_2CO_3}$ and $\mathrm{K_2CO_3}$, since the ionic asymmetry combines with the system anisotropy at the interface to affect the structure and dynamics of the interfacial layers. More details on this analysis are given in the Supplemental Information.

The slow diffusion of ions along z at the interface suggests that their motion could be described in terms of hopping among the several well defined layers that can be seen in the density profiles of our samples. To verify this picture, we identify once again and label all the ions residing in the first density layer. For each of these ions we measure the time elapsed before it jumps to another layer. Jumps are disregarded if the hopping ion returns to the first layer within 0.1 ps. This analysis is repeated many times along each trajectory to average over the initial instant of time. The distribution of times to the first jump $p_j(t)$ is indeed fairly exponential (see Fig. YY in SI), as expected for the rare hopping of particles among distinct free energy valleys separated by sizeable activation barriers. The time constants τ ($P_j(t) = A \exp[-t/\tau]$) for all species and temperatures are reported in Tab. XI. At the relatively high temperature of our simulations, however, the exponential time constant is relatively short, somewhat undermining the discrete hop picture. Because of these contradicting considerations, we leave open the question on whether hopping between planes is a relevant picture for the dynamics of ions perpendicular to the interface, where density oscillations are important.

A single simulation has been performed for the $LiNaCO_3$ mixture, partly because of its interest for MCFC, but especially to see how the Li^+ and Na^+ ions position themselves relative to the interface. The simulation started from a random distribution of Li and Na ions, and lasted 2 ns after an equilibration run of 1.2 ns, with a target temperature of $T = 1300$ K. Figure 11 reports the difference in the Li^+ and Na^+ concentrations along z. It turns out that Li^+ and Na^+ ions are nearly equally represented in the first layer at contact with the solid-like wall. However, because of its smaller size, Li^+ ions reach closer to the wall than Na^+ ions, giving a characteristic but rather irrelevant high-amplitude, high-frequency oscillation to the concentration profile at contact.

Figure 11 also shows a long wavelength fluctuation of the Li^+ and Na^+ relative concentration, whose amplitude, however, is fairly small, and decreases (slowly) with increasing simulation time. Since the analysis of homogeneous $LiNaCO_3$ mixtures provided evidence of full miscibility of Li_2CO_3 and Na_2CO_3, we think that this oscillation is simply the result of a statistical fluctuation, whose relaxation time is long. The long relaxation time, in turn, is consistent with the long-wavelength limit of $S_{cc}(k)$ briefly discussed in the previous subsection.

Last but not least, we investigated the range of correlations in our inhomogeneous samples, to validate or disprove early speculations on the power-law decay of distribution functions parallel to the interface. The result for Li_2CO_3 at $T = 1300$ K is shown in Fig. 12. The proximity of the interface greatly enhances the amplitude, and conserves the wavelength and phase of the oscillating decay of bulk distribution functions. The envelop, however, is exponential in both cases, implying short range correlations also parallel to the interface.

The dipole of each interface, D_{left} and D_{right}, were calculated from the charge density, ρ_Q, by the use of the following equations:

$$D_{left} = \int_{-L_z/2}^{0} z\rho_Q(z)dz \tag{21}$$

$$D_{right} = \int_{0}^{L_z/2} z\rho_Q(z)dz \tag{22}$$

Given the equivalence of the left and right interfaces at equilibrium, these two values should be equal in magnitude and of opposite sign. Small deviations due to statistical errors, however, might occur. To improve statistics, we average over the two opposite dipoles.

As already stated, in our protocol the simulation was done in stages. Each stage consisted of 10^5 steps, i.e. 0.1 ns. The first two stages were used for equilibration. The remaining 8 stages was divided into 4 blocks, e.g. stage 3 and 4 becomes one block, 5 and 6 another one and so on. The electrostatic dipole of each interface was averaged for each block.

To get the dipole, for each block an average was taken of $|D_{left}|$ and $|D_{right}|$. Thus for each system, four values were acquired for the dipole. These were averaged to give the values seen in Table XIII. The error bar was computed as 2 times the standard deviation of the four values and then divided by $\sqrt{N}$, where N is the number of blocks.

The simulation of Li_2CO_3 at 1300 K and 1500 K where run up to 1.4 ns, meaning six blocks were used for production instead of four.

The electrostatic potential difference ψ_s between the walls and the centre of the slab (bulk M_2CO_3) is directly proportional to the interfacial dipole moment. The value of ψ_s is shown in Tab. XIII. By construction, these values represent the potential of zero charge (ψ_{pzc}) for the model interface.

As expected, the magnitude of the interfacial dipole increases monotonically with increasing asymmetry between cation and anion, as can be seen in Tab. XIII.

The same table shows that the interfacial dipole increases with temperature, although the relatively large error bar prevents us from verifying that $\mid D \mid$ is a strictly monotonic function of temperature. However, the results available from the literature for idealised models of simple spherical ions confined by structureless walls show a similar increase of the dipole with increasing temperature,[24] enhancing our confidence in this result. Moreover, the increase of the dipole magnitude with increasing T could be interpreted as due to a decreasing ability of the electrolyte to screen the strong perturbation represented by the metal wall, and, in this sense, it is also consistent with simple analytical theories such as Poisson-Boltzmann[90] and Debye-Hückel.[91] The experimental picture is far more complex (see Trasatti, Ref. 94), reflecting the huge variety of interfaces between metals and electrolytes.

Besides the electrostatic potential of zero charge, a second crucial parameter for any electrified interface is the interfacial capacitance.

For a planar interface, this is directly related to the fluctuations of the instantaneous dipole moment,[93] according to:

$$\frac{1}{C_D} = \frac{\partial D}{\partial \sigma} = -4\pi\beta \left[\langle D^2 \rangle - \langle D \rangle^2\right] \tag{23}$$

where σ is the surface charge, and D is either D_{left} or $-D_{right}$. A correction is introduced by the usage of periodic boundary conditions,[89] and by the (particle-particle particle-mesh) Ewald approach to account for long range Coulomb interactions. This further contribution, however, is small, and it is further reduced by the electro-neutrality of the wall in our simulations. For this reason, we estimate the capacitance through Eq. 23.

As already stated, the particles belonging to the solid-like wall are neutral. Despite the asymmetry of cations and anions, the surface dipole is small and difficult to compute with an acceptable relative accuracy. The fluctuations of the dipole, instead, are large, and the computation of $\langle D^2 \rangle - \langle D \rangle^2$ can be carried out fairly quickly with a relative error of the order of a percent. The results are given in Tab. XIV.

The capacitance measures how easy it is to change the interfacial charge upon changing the electrostatic potential. The values in Tab. XIV show that the capacitance decreases with increasing asymmetry of the ions, possibly because the local charge distribution of highly asymmetric systems makes it difficult to add further charge to an already polarised interface.

The dependence of capacitance on temperature is an additional important issue. The data in Tab. XIV show that C_D increases with increasing T. This agrees both with idea that the capacitance is the inverse of an electrostatic rigidity of the interface, and with the available experimental data.[95]. Computations for idealised models of solid/molten salt interfaces in most cases fail to reproduce this interesting feature.

C. Charged interfaces

To verify the qualitative validity of our estimates of the interfacial capacitance, we carried out a single computation for Li_2CO_3 at $T = 1300$ K in which the particles representing metal atoms carry an electrostatic charge of ±0.1e on the left and right solid wall, respectively. This corresponds to a surface charge $\sigma = (0.3)$ C/m^2, that is fairly high for real systems. The periodicity of the charge distribution along z, however, reduces the surface electric field by a factor of ... with respect to the planar capacitor value. The renormalised electric field corresponds to a surface charge of .. C/m^2,or .. e/nm^2, that we take as the true surface charge of the simulated interfaces. Also in this case simulations lasted 1 ns, covered in steps of 1 fs. This relatively short time span is probably more adequate for charged interfaces than for neutral systems, since the surface charge enhances the coupling of the solid wall with the fluid, speeding up relaxation.

The charge density profiles is shown in Fig. 14, while the number or mass density profiles (not shown) are almost indistinguishable from the neutral wall case.

The corresponding electrostatic potential at the two interfaces is shown in Fig. 15.

Because of the inherent asymmetry in the cation and anion species, and, even more, because of the non-linearity in the electrostatic response of the fluid, the variation of the electrostatic potential from the zero charge value is slightly different at the two interfaces. However, the estimate of the interface capacitance, computed as:

$$\frac{1}{C_D} = \frac{[\psi(+\sigma) - \psi(-\sigma)]}{2\sigma} \tag{24}$$

where $\sigma =$ .. is the surface charge renormalised by pbc, turns out to be compatible with the value obtained from the simulation at zero electrode charge.

The simulation of charged interfaces has not been extended much further in our study because the limitations of the model do not warrant a larger scale effort.

IV. SUMMARY AND CONCLUSIONS

Molten alkali carbonates represent the electrolyte of choice for a wide variety of electrochemical devices, and, in particular, for molten carbonate fuel cells (MCFC) that are being developed and to some extent deployed to enhance the efficiency and decrease the environmental impact of electric power generation.

Moreover, molten alkali carbonates are among the simplest molecular liquid salts. Despite their relatively high melting point, they could play an important role to spearhead the development of devices based on molecular electrolytes of increasing complexity and lower melting point, exemplified by the so called room temperature ionic liquids.[5]

To enhance our understanding of these systems, we carried out an extensive investigation of molten alkali carbonates Li_2CO_3, Na_2CO_3, K_2CO_3 and $LiNaCO_3$ using molecular dynamics simulation based on a thoroughly tested empirical force field.[22,23] For reasons of computational convenience, the model does not explicitly include atomic polarisability.

To verify and extend the several studies carried out by other groups using similar models and methods, we first performed simulations for homogeneous systems made of 512 molecules at temperatures $1200 \leq T \leq 1500$ K, under a moderate overpressure of 15 kbar to compensate for a systematic underestimate of the equilibrium density by the JT force field.

Since electrochemical devices usually involve the interface between the electrolyte and an electronic (metal) conductor, we also simulated inhomogeneous systems in which a thick slab of molten carbonates is confined between two thin layers of *neutral* atoms tethered to a compact hexagonal 2D lattice, whose geometric parameters reproduce those of the (111) surface of gold. The solid wall model is still very idealised, since it does not include image charges, it is atomistically thin, and its interaction with the carbonate ions is described by pair potentials, that are certainly inadequate for metal surfaces. Nevertheless, it introduces a particle-based representation of the solid electrode, and, in this respect, it represents an important step forwards with respect to previous simulations adopting structures-less, neutral or charged rigid walls. Moreover, the springs tethering solid particles to the underlying rigid 2D lattice re-introduce the effect of surface elasticity, which could be tuned to mimic different solid materials.

The results could be described as follows.

Our simulations of homogeneous systems largely agree with those of previous studies based on unpolarisable force fields. We find, in particular, that simulation results reproduce the few experimental data available in the literature on the atomistic structure of molten alkali carbonates, including details of the first coordination shell, as well as scattering properties as described by various combinations of the partial structure factors. Equimolar $M_1M_2CO_3$ mixtures, relevant to model eutectics used in applications, tend to behave as ideal mixtures. Local fluctuations of composition relax very slowly to the homogeneous equilibrium state, probably because of the low free energy driving force, coupled to the relatively low diffusion constant of all species.

On the other hand, the model tends to underestimate transport coefficients such as the diffusion coefficient, the electrical conductivity, and, perhaps, the heat conductivity. It is important to notice, however, that also the experimental data suffer from limitations in their accuracy, with error bars no better than 10 %. Despite these drawbacks, simulation fully confirms that diffusion, conductivity and heat transfer are predominantly due to cations, contrary to early speculations attributing a special role to anions.[87] Moreover, the model displays a remarkable enhancement of electrical conductivity with respect to the Nernst-Einstein (NE) value based on diffusion. This contradicts the usual interpretation of deviations from NE as due to ion pairing, and we propose that it could be due to back-flow, i.e., a many body effect introduced a few decades ago to explain correlation and dynamics in the interacting electron gas.[83]

The simulation of inhomogeneous systems made of molten carbonates confined by parallel, planar walls represents the most original and most important part of the present study. Systems of 2048 molecular units are simulated in an orthorhombic cell of 36.047 × 36.7038 Å cross section, and length in all cases exceeding 100 Å . Basic thermodynamic properties such as density of the bulk phase far from the interface and the interface absorption of cations and anions are computed from simulation trajectories. We also determine and report number density and electrostatic charge density profiles perpendicular to the solid-like wall, displaying characteristic oscillations whose envelop decays exponentially moving towards the centre of the slab. Needless to say, the robust oscillations seen in all simulation profiles contradict the monotonic screening predicted by time honored theories such as Debye-Hückel and Poisson-Boltzmann, and agree at least qualitatively with the results of integral equation theories such as RISM.[97]

We analysed density and charge correlations along the interfacial plane, and found that oscillations in the correlation functions are greatly enhanced with respect to the bulk. The decay of correlation functions with increasing distance, however, remains exponential, contrary to the conclusions of statistical mechanics studies.

As expected, the presence of the interface greatly affects dynamical properties. Diffusion, for instance, is highly anisotropic close to the solid wall, being faster along the interfacial plane than in the orthogonal direction. Even along the parallel plane, diffusion is slower in the vicinity of the interface than in the middle of the slab. To model the slow diffusion in the direction perpendicular to the interface, we developed and tested a simple hopping picture for the motion of ions among density planes adjacent to the solid wall, which might indeed capture a few qualitative features of the ion dynamics at interfaces.

Electrochemistry applications, of course, rely primarily on cations and anions to carry out reactions and to transport charge and energy across the system. To investigate these properties, we computed the electrostatic dipole moment of each interface, which, for walls made of neutral particles, is proportional to the potential of zero change of our model. The simulation results show that the dipole as well as the zero-charge potential increase with increasing temperature, although the error bar prevents us from verifying whether their dependence on T is monotonic. Despite fairly large error bars, our confidence in this observation is supported by the results of idealised models based on simple (i.e., made of isotropic point particles) Coulomb fluids, and we think that it reflects the decreasing ability with increasing T of the fluid to screen the presence of the wall. The importance of all these effects depends on the choice of the M_2CO_3 fluid, since the dipole moment an ψ_{zpc} for a neutral wall greatly depend on the size asymmetry of cations and anions.

Finally, we computed the interfacial capacitance at the point of zero charge, using both a fluctuation-based formulation, and a finite difference expression whose evaluation required the simulation of charged interfaces. The results of the two computational approaches are consistent with each other. Using the fluctuation route for neutral interfaces, we found that the interfacial capacitance decreases with increasing asymmetry of the ions, and increases with increasing temperature. This last result, in particular, agrees with experimental data for simple molten salts, and differs from the results of more idealised models all based on unpolarisable ions and rigid solid walls.

The simulation study presented in this paper provides a detailed and vivid picture of the interplay of packing, correlation and electrification effects at interfaces between solid walls and molecular ionic fluids. To the best of our knowledge, only a few other studies of similar interfaces have been reported in the literature (we explicitly exclude simulations of more complex interfaces relevant for Li batteries). Given the huge number and variety of molecular molten salts, and, even more, given the current interest in ionic conductors at moderate temperature, we expect a rapid growth of computational studies devoted to these systems, that could greatly expand our understanding of complex interfaces, and ease the development of electrochemical devices.

To achieve these aims, however, more realistic models are needed, including polarisation, and perhaps based on ab-initio methods.

Needless to say, simulations of systems under non equilibrium conditions such as those corresponding to the steady state transport of heat, current or mass are more challenging than equilibrium simulations, and highly valuable for electrochemical applications. The information from the present study offers the opportunity to estimate the time required, for instance, to compute the Seebeck coefficient of cells consisting of molten alkali carbonates confined by two metal walls at different temperature. In practice, computing the Seebeck coefficient requires computing the dipole moment across a cell in which a thermal gradient drives the steady state transport of heat. In the experiments by Børset et al. Ref. 17, the temperature difference between the electrodes were smaller than 20 K in order to avoid non-linearity corrections in the Seebeck coefficient. Based on the results of our simulation for D, taking into account the slow decay of statistical error bar δ with increasing simulation time t ($\delta \sim t^{-1/2}$) we estimate that a quantitative determination of the Seebeck coefficient for alkali carbonates under realistic conditions will take simulations covering a few μs that could be carried out with a large but feasible computational effort.

ACKNOWLEDGEMENTS - Computations have been carried out on the NOTUR supercomputers.

Supporting information: - Optimised geometry of the neutral ion pairs; ESP charges of cations, anions and neutral pairs; vibrational eigenvectors and infrared activity of harmonic modes for all neutral ion pairs; discussion of similarities and differences between ab-initio and force field modelling. This material is available free of charge via the Internet at http://pubs.acs.org.

V. APPENDIX

The JT potential used in our study and in several other recent computational investigations of molten alkali carbonates has been constructed by fitting a standard analytical form on the results of Hartree-Fock (HF) computations for single carbonate ions bound to zero, one and two alkali cations. Since HF is no longer a popular approach in electronic structure computations, we carried out similar total energy computations comparing the results of HF, and of closely related density functional approximations of the generalised gradient (PBE?) and of the hybrid (B3LYP?) type. For each exchange-correlation (XC) approximation, we computed ground state geometry, total energy, vibrational frequencies and Mulliken charges for Li_2CO_3, Na_2CO_3, K_2CO_3, and closely related species. Carbonic acid H_2CO_3 has been added to the short list of bona fide alkali-carbonates because several computational studies have been published on this molecule, whose existence in the gas phase is uncertain at best.

Detailed tables with all the data are given as supporting information. Here we summarise the results relevant for our study.

First of all, we point out that, strictly speaking, no method among those we considered is able to deal with the gas-phase CO_3^{2-} anion since at least a few of the HF or Kohn-Sham eigenvalues for the occupied states turn out to be positive (see Table in Supporting Information), implying that the corresponding orbital is not localised. The accepted practice in quantum chemistry is to disregard this problem of principle, since the localised Gaussian basis used in our (and similar) computations prevents the electron density to spread far from the ion, and the potential energy obtained in this way is usually good enough for the interpretation of basic thermochemistry data.

We adopt this pragmatic point of view, but we think important to realise that ab-initio approaches are exact only in their idealised version, while in practical implementations they involve many approximations and display important limitations.

With this note of caution, the results of our HF and DFT computations are as follows. First of all, the geometry of the carbonate ion, and of all the other species considered in our ab-initio computations depends very little on the exchange-correlation approximation. Somewhat more surprising, also the energies to dissociate M_2CO_3 into ions are not so sensitive to XC, and also vibrational frequencies are again rather insensitive to the XC part.

From all these points of view, therefore, the HF data are nearly as good as those of higher level computations.

On the other hand, we observe that the out of planarity deformations of CO_3^{2-} has a frequency of at least 800 cm^{-1}, that corresponds to an energy of $\sim 10^3$ K, suggesting that the out of plane flexibility of this ion might play a role at the temperatures of our simulations. Bending, and, even more, stretching have higher frequencies, and are effectively frozen at realistic temperatures. Their freezing by a constraint cannot affect much the results, including, for instance, the self-diffusion constant.

Besides these general considerations, we remark a few more delicate features. First of all, the ground state CO_3^{2-} moiety in M_2CO_3 doesn't have D3h symmetry, but, rather C2v, since the C-O1 distance is different from C-O2 and C-O3 (see Fig. 1). Needless to say, O1, O2 and O3 are in principle equivalent in CO3mm, and only their position with respect to the metal atoms differentiates their bond to C.

No standard model is able to reproduce the symmetry and bonding dependence of CO_3^{2-} on metal ion coordination. Since these effects arise from redistribution of electronic charge, we might attribute them to electronic polarisation effects. However, it might be easier to see them as environment-dependent effects that are more naturally covered by bond-order potentials. The charge equalisation method used in Ref. 55 is another approach able to overcome this problem, and the method is non included in most simulation packages.

---

[1] M. P. Tosi and F. G. Fumi, J. Phys. Chem.Solids **25**, 45 (1964).

[2] L. V. Woodcock and K. Singer, Trans. Faraday Soc. **67** 12-30 (1971).

[3] B. Larsen, T. Forland, K. Singer, Mol. Phys. **26**, 1521-1532 (1973).

[4] D. J. Adams and I. R. McDonald, J. Phys. C: Solid State Phys. **7** 2761 (1974).

[5] Welton, T. *Chem. Rev.* **1999**, *99*, 2071.

[6] F. T. Mackenzie, Carbonate mineralogy and geochemistry, in *Encyclopedia of Earth Science: Sedimentology*, Springer pp 147-158 (2003).

[7] F. Gaillard, M. Malki, G. Iacono-Marziano, M. Pichavant, and B. Scaillet, Science **322**, 1363 (2008).

[8] Dasgupta, R.; Hirschmann, M. M. Earth Planet Sci. Lett. **298** 1-13 (2010).

[9] A.P.Jones, M. Genge, L. Carmody, Rev. Mineralogy Geochemistry **75**, 289 (2013).

[10] G. J. Janz, *Molten Salts Handbook*, (Academic Press, New York, 1967).

[11] Ward, A. T., and Janz, G. J. (1965). Molten carbonate electrolytes: electrical conductance, density and surface tension of binary and ternary mixtures. Electrochim. Acta 10, 849–857. doi:10.1016/0013-4686(65)80048-2

[12] Cassir, M., McPhail, S., and Moreno, A. (2012). Strategies and new developments in the field of molten

[13] Dicks, A. L. Curr. Opinion in Solid State and Mat. Sci. **8**, 379-383 (2004). carbonates and high-temperature fuel cells in the carbon cycle. Int. J. Hydrogen Energy 37, 19345. doi:10.1016/j.ijhydene.2011.11.006.

[14] K. Xu, Chem. Rev. **114**, 11503-11618 (2014).

[15] D. Chery, V. Lair, and M. Cassir, Front. Energy Res. **3**:43, doi: 10.3389/fenrg.2015.00043.

[16] Suguira, K., Takei, K., Tanimoto, K., and Miyazaki, Y. (2003). The carbon dioxide concentrator by using MCFC. J. Power Sources 118, 218–227. doi:10.1016/S0378-7753(03)00084-3

[17] Børset, M. T.; Kang, X.; Burheim, O. S.; Haarberg, G. M.; Xu, Q.; Kjelstrup, S., Electrochimica Acta **182**, 699-706 (2015).

[18] Licht, S.; Wang, B.; Ghosh, S.; Ayub, H.; Jiang, D.; Ganley, J.A New Solar Carbon Capture Process: Solar Thermal Electrochemical Photo (STEP) Carbon Capture J. Phys. Chem. Lett. 2010, 1, 2363-2368, DOI: 10.1021/jz100829s

[19] *Modern Electrochemistry, 2nd ed.* - M. Bockris, N. Reddy, Kluwer Accademic, (2000).

[20] J.A. Plambeck, Fused Salt Systems, Vol. X of Encyclopaedia of Electrochemistry of the Elements, M. Dekker, New York and Basel, 1976.

[21] Kojima, T., Miyazaki, Y., Nomura, K., and Tanimoto Density, K. (2008). Surface tension, and electrical conductivity of ternary molten carbonate system Li2CO3-Na2CO3-K2CO3 and methods for their estimation. J. Electrochem. Soc. 155, F150–F156. doi:10.1149/1.2917212

[22] G. J. M. Janssen and J. T. W. M. Tissen, Mol. Sim. **5**, 83-98 (1990).

[23] J. T. W. M. Tissen and G. J. M. Janssen, Mol. Phys. **71**, 413-426 (1990).

[24] D. Henderson and D. Boda, Phys. Chem. Chem. Phys. **11**, 3822-3830 (2009).

[25] C. Pinilla, M. G. Del Pópolo, J. Kohanoff, and R. M. Lynden-Bell, J. Phys. Chem. B **111**, 4877-4884 (2007).

[26] C. Merlet, B. Rotenberg, P. A. Madden, M. Salanne, Phys. Chem. Chem. Phys. 2013, 15, 15781-15792.

[27] E. Peled, J. Electrochem. Soc. **126** 2047-2051 (1979).

[28] R. Jorn, R. Kumar, D. P. Abraham, and G. A.Voth, J.Phys. Chem. C **117**, 3747-3761 (2013).

[29] Kevin Leung

[30] D. Bedrov, G. D. Smith, A. C. T. van Duin, J. Phys. Chem. A **116**, 2978-2985 (2012).

[31] J. B.Bates, M. H. Brooker, A. S. Quist, and G. E.Boyd, J.Phys. Chem. **76**, 1565 (1972).

[32] Koura N, Kohara S, Takeuchi K, Takahashi S, Curtiss L A, Grimsditch M and Saboungi M-L

1996 J. Mol. Struct. 382 163.

[33] H. Ohno, X-Ray Diffraction Analysis of Structure of Ionic Liquids, JAERI memo 63-221, June 1988. Results reported in Ref. 35

[34] J. Zarzycki, Discuss. Faraday Soc., 32 (1961) 38. J. Phys.: Condensed Matter **10**, 3301(1998).

[35] Kohara, S.; Badyal, Y. S.; Koura, N.; Idemoto, Y.; Takahashi, S.; Curtiss, L. A.; Saboungi, M.-L., J. Phys. C: Condensed Matter **10**, 3301-3308 (1998).

[36] Mills, R.; Spedding, P. L. J. Phys. Chem. **70**, 4077 (1966).

[37] Spedding, P. L.; Mills, R. J. Electrochem. Soc. **112**, 594 (1965).

[38] Janz, Bansal,

[39] S. Otsubo, T. Nozaki, Y. Nagasaka, A. Nagashima High Temperatures high Pressures **29**, 201-206 (1997).

[40] Y. Nagasaka, in: *Experimental Thermodynamicsi (Vol. 9): Advances in Transport Properties of Fluids*, Edited by: M. J. Assael, A. R. H. Goodwin, V. Vesovic, W. A. Wakeham, Royal Society of Chemistry, London, (2014).

[41] Nunes, V. M. B. and Lourenço, M. J. V. and Santos, F. J. V. and de Castro, C. A. N., J. Chem. Eng. Data, **48**, 446-450, (2003).

[42] Egorov, B.N.; Revyakina, M. P. High temperature , 1970, Vol.8(6), p.1220.

[43] G. J. Janz and M. R. Lorenz, J. Electrochemical Soc. **108**, 1052 (1961).

[44] Cowley, E. R.; Pant, A.K. Lattice dynamics of calcite, Phys. Rev. B **8** 4795 (1973).

[45] A. Pavese, M. Catti, G. D. Price, R. A. Jackson, Phys. Chem.Minerals **19**, 80-87 (1992).

[46] Dove, M.T.; Winkler, B.; Leslie, M.; Harris, M. J.; Salje, E. Am. Min. **77**, 244-250 (1992).

[47] Duan, Y.; Sorescu, D. C. Phys. Rev. B **79** 014301 (2009).

[48] Shang, S.-L.; Hector, L. G. Jr.; Shi, S.;Qi, Y.; Wang, Y.; Liu, Z.K. Acta Materialia **60**, 5204-5216 (2012).

[49] Ricca, C.; Ringuedé, A.; Cassir, M.; Adamo, C.; Labat, F. Surf. Sci. **647**, 66-77 (2016).

[50] Tomczyk, P. J. Electroanal. Chem. **379**, 353-360 (1994).

[51] Janowitz, K.; Kah, M.; Wendt, H. Electrochim. Acta **45**, 1025-1037 (1999).

[52] J. Habasaki, Mol. Phys. **69**, 115-128 (1990).

[53] D. Corradini, F.-X. Coudert, and R. Vuilleumier, J. Chem.Phys. **144**, 104507 (2016).

[54] Čančarevič, Ž., Schön, J. C. and Jansen, M. (2006), Alkali Metal Carbonates at High Pressure. Z. Anorg. Allg. Chem., 632: 1437–1448. doi:10.1002/zaac.200600068.

[55] M. F. Costa and M. C. C. Ribeiro, J. Mol. Liq. **138**, 61 (2008); errata: *ibid.* **142**, 161 (2008).

[56] P. Raiteri, R. Demichelis, and J. D. Gale, J. Phys. Chem. C, **119**, 24447-24458 (2015).

[57] R. Demichelis, P. Raiteri, J. D. Gale, D. Quigley and D. Gebauer, Nat. Commun. **2**, 590 (2011).

[58] Wilding, M. C.; Wilson, M.; Alderman, O. L. G; Benmore, C.; Weber, J. K. R.; Parise, J. B.; Tamalonis, A.; Skinner, L., Scientific Reports **6**, xxx (2016).

[59] M. Masia, M. Probst, and R. Rey, J. Phys. Chem. B **108**, 2016-2027 (2004).

[60] Ottochian, A.; Ricca, C.; Labat, F.; Adamo, C. Molecular dynamics simulations of a lithium/sodium carbonate mixture, J. Molecular Modelling **22**, 1-8 (2016).

[61] Bhargava, B. L.; Balasubramanian, S. J. Chem. Phys. 2007, 127, 114510-114516

[62] Ryckaert, J. P.: Ciccotti, G.; Berendsen, H. J.; J. Comput. Phys. **23**, 327-341.

[63] M. S. Daw and M. I. Baskes, Phys. Rev. Lett. **50**, 1285 (1983).

[64] M. I. Baskes, Phys. Rev. Lett. **59**, 2666 (1987).

[65] Shelley, J. C.; Bérard, D. R. In Reviews in Computational Chemistry, Vol. 12; Lipkowitz, K. B.; Boyd, D. B. Eds.; Wiley: New York, 1998.

[66] Iori, F.; Corni, S. J. Comput. Chem. 2008, 29, 1656.

[67] D. Frenkel,

[68] J. W. Eastwood, R. W. Hockney, D. N. Lawrence, Computer Physics Communications 19 (1980) 215-261

[69] Arnold, A. and Holm, C., J. Chem. Phys. **123**, 144103 (2005).

[70] Arnold, A. and Holm, C., Computer Phys. Commun. **148**, 327-348, (2002).

[71] Arnold, A. and de Joannis, J. and Holm, C., J. Chem.Phys. **117**, 2496-2502 (2002).

[72] S. Plimpton, Fast Parallel Algorithms for Short-Range Molecular Dynamics, J Comp Phys, 117, 1-19 (1995).

[73] K.Motzfeldt, J.Phys. Chem. **59**, 139-147 (1955).

[74] Koishi, T. and Kawase, S. and Tamaki, S. and Ebisuzaki, T. Computer Simulation of Molten $Li_2CO_3-K_2CO_3$ Mixtures, J. Phys. Soc. Japan, 69, 3291-3296 (2000).

[75] Hansen, J.-P. and McDonald, I. R. *Theory of Simple Liquids*, Elsevier, Amsterdam (2006).

[76] Ohata, H.; Takeuchi, K.; Ui, K.; Koura, N., ECS Transactions **6**, 57-65 (2007).

[77] Spedding, P. L. and Mills, R-, J. Electrochem. Soc. **112**, 594-599 (1965).

[78] Zhang, X.; Fujii, M., Int. J. Thermophysics **21**, 71-84 (2000).

[79] Armstrong, J. A.; Ballone, P. J. Phys. Chem. B **115** 4927-4938 (2011).

[80] Trullas, J. and Padró, J. A., Phys. Rev. B **55**, 12210 (1997).

[81] Tasseven, Ç.; Trullas, J.; Alcaraz, O.; Silbert, M.; Giró, A. J. Chem. Phys. **106**, 7286-7294 (1997).

[82] Yamaguchi, T.; Nagao, A.; Matsuoka, T.; Koda, S., J. Chem. Phys. **119** 11306-11317 (2003).

[83] Pines, D. and Nozieres, P. *Theory of Quantum Liquids: Normal Fermi liquids*, Addison-Wesley, Boston (1989).

[84] Jancovici, B. J. Stat. Mech. **28**, 43-65 (1982).

[85] F. A. Cotton, J. Wilkinson, C. A. Murillo, M. Bochmann, Advanced Inorganic Chemistry, Sixth Edition Wiley, 1999

[86] H. Näfe, ECS Journal of Solid State Science and Technology, **3**, N7-N14 (2014).

[87] T. F. Fuller, Electrochem. Soc. Interface, 146, 872 (1997).

[88] Stillinger Lovett

[89] Ballone, P.; Pastore, G.; Tosi, M. P. J. Chem. Phys. 85, 2943-2950 (1986).

[90] A reference on Poisson Boltzmann

[91] P. W. Debye and E. Hückel, Phys. Z. **24**, 185 (1923).

[92] G. Bilalbegović, F. Ercolessi, E. Tosatti Surf. Sci. 280, 335-348 (2003).

[93] L. Blum, O. Henderson, J. L. Lebowitz, C. Gruber, and P. A. Martin, J. Chem. Phys. 75, 5974 (1981).

[94] Comprehensive Treatise of Electrochemistry, Vol. 1, J. O'M. Bockris, B. E. Conway, and E. Yeager, eds., Plenum Press, New York, 1980.

[95] A. D. Graves, J. Electroanal. Chem. 25 (1970) 349, 357.

[96] R. D. Shannon (1976). "Revised effective ionic radii and systematic studies of interatomic distances in halides and chalcogenides". Acta Crystallogr A. 32: 751-767.

[97] Fedorov

Figures

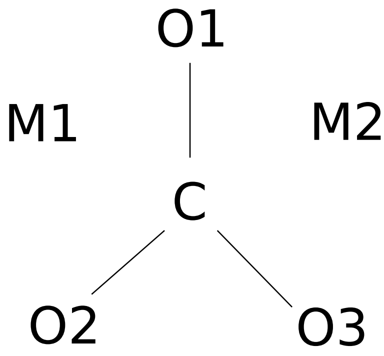

FIG. 1: Schematic of M_2CO_3, where M is either Li, Na, K or H.

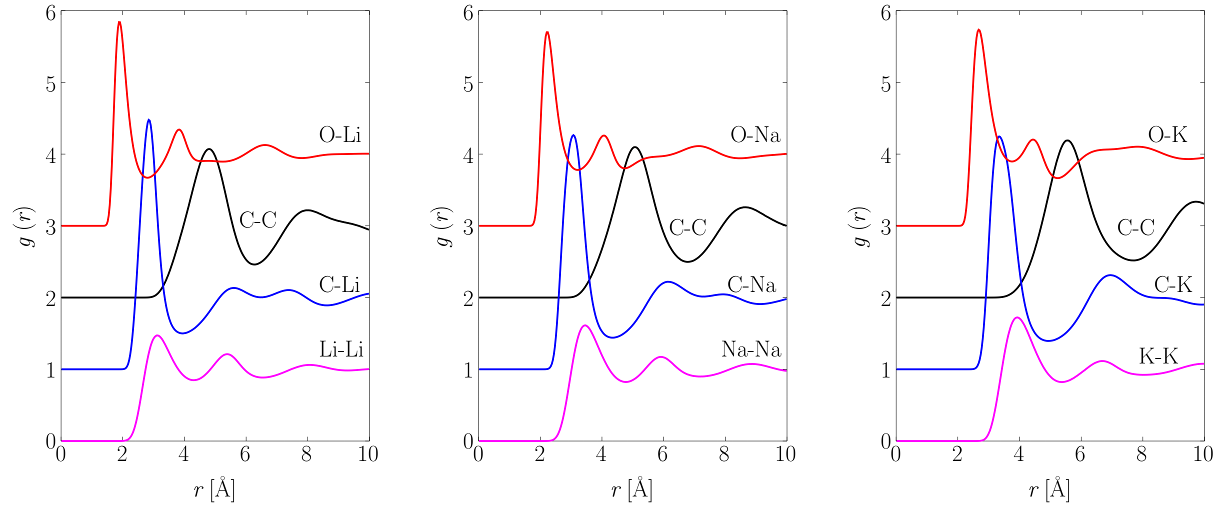

FIG. 2: Radial distribution function for Li_2CO_3 (left), Na_2CO_3 (middle) and K_2CO_3 (right) at $T = 1200$ K, $P = 15$ kbar. All the curves, except the bottom one, have been shifted for readability.

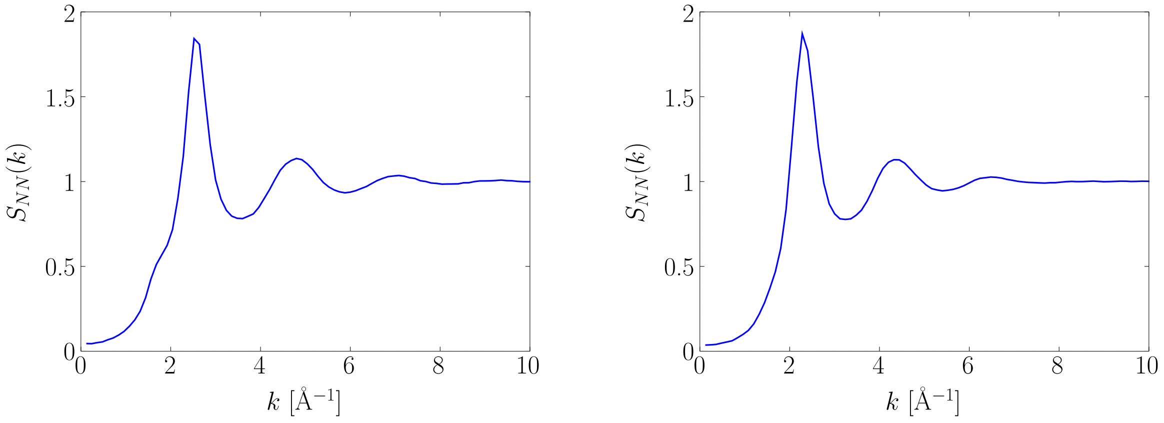

FIG. 3: Number structure factor as a function of wavenumber for Li_2CO_3 (left) and Na_2CO_3 (right) at $T = 1200$ K, $P = 15$ kbar.

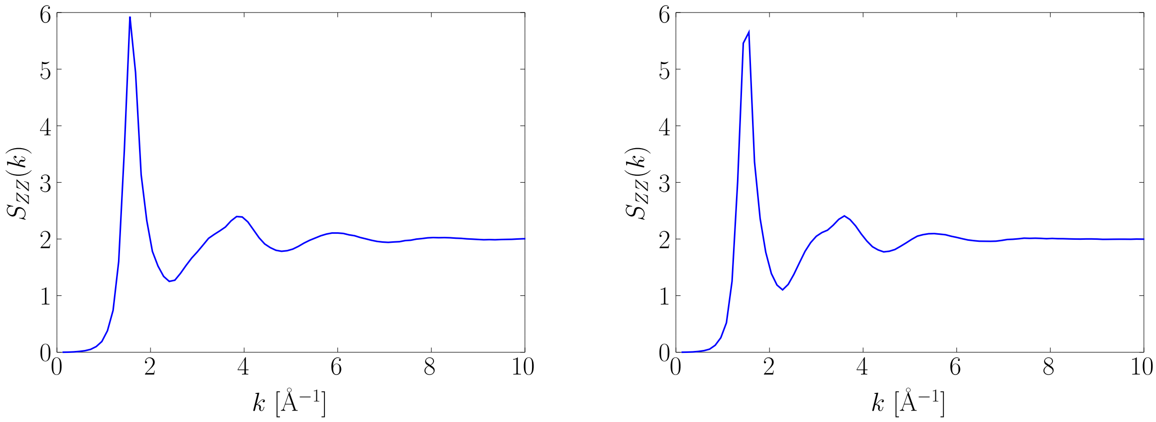

FIG. 4: Charge structure factor as a function of wavenumber for Li_2CO_3 (left) and Na_2CO_3 (right) at $T = 1200$ K, $P = 15$ kbar.

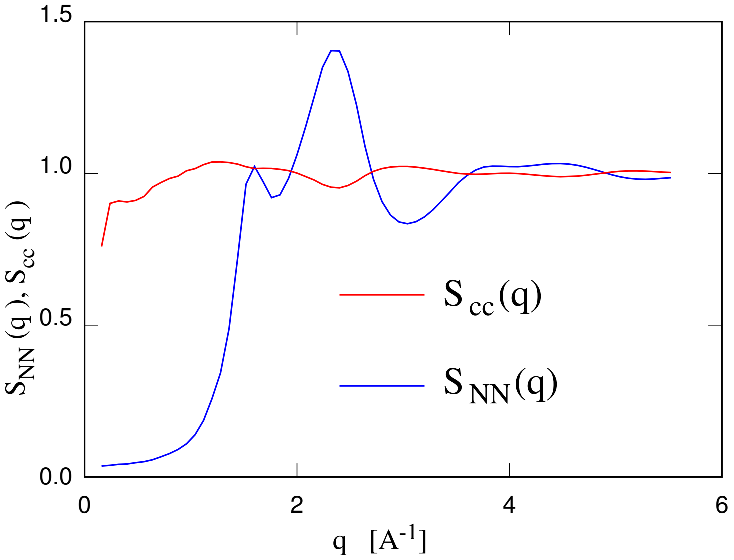

FIG. 5: Concentration-concentration structure factor of Li^{+} and Na^{+} ions in the $LiNaCO_3$ liquid mixture at $T = 1300$ K.

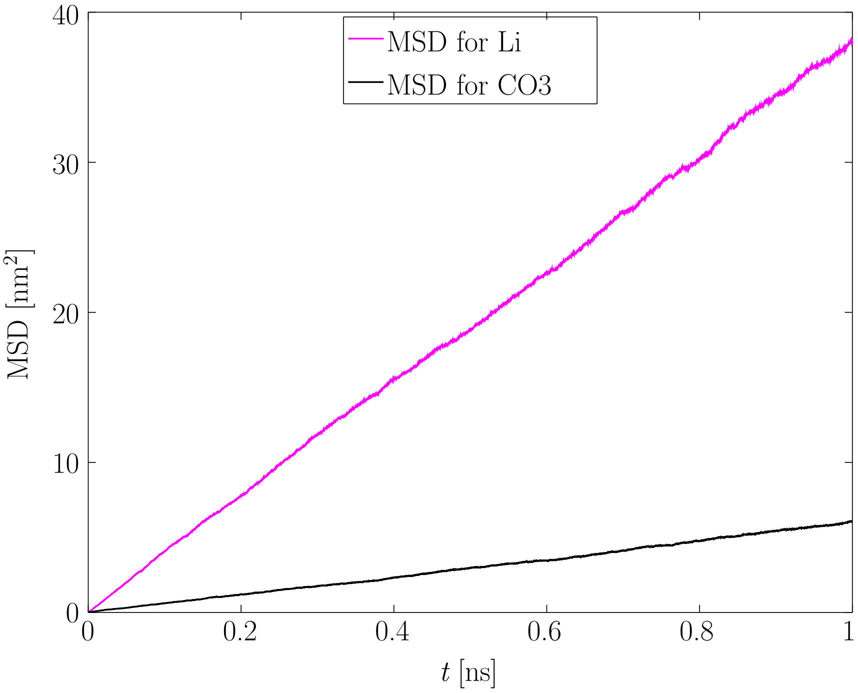

FIG. 6: Mean square displacement for Li_2CO_3 at $T = 1200$ K, $P = 15$ kbar.

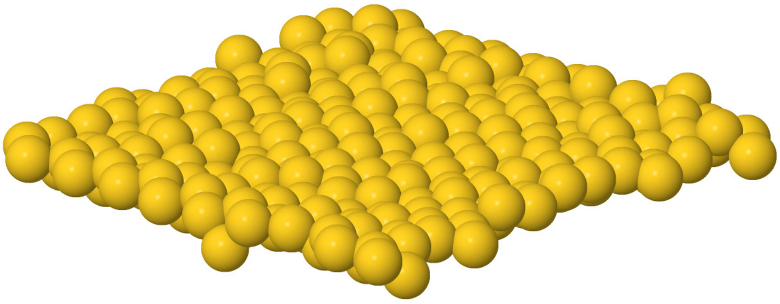

FIG. 7: Snapshot of the tethered particles' layer mimicking the metal electrode layer at high temperature. Particle sizes are tuned on gold atoms, see Ref. 66

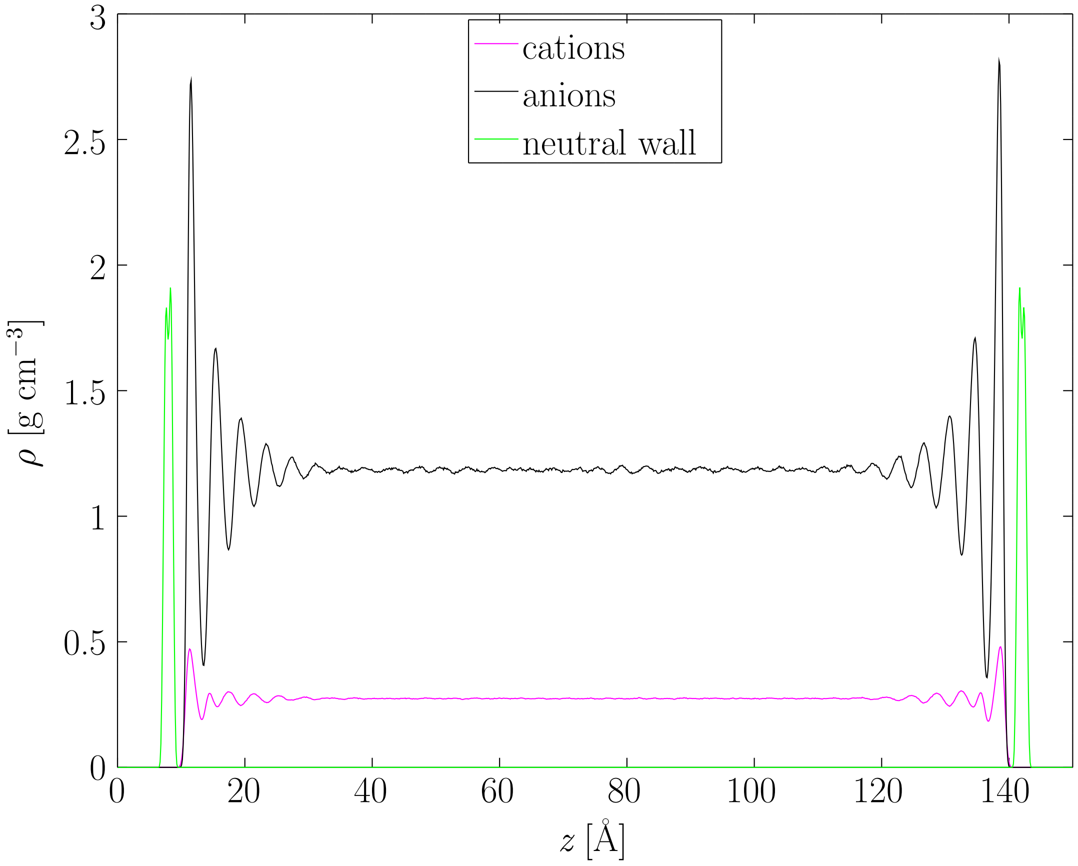

FIG. 8: Density profile for anions, cations and neutral particles from the simulation of Li_2CO_3 confined between two planar neutral walls at 1300 K.

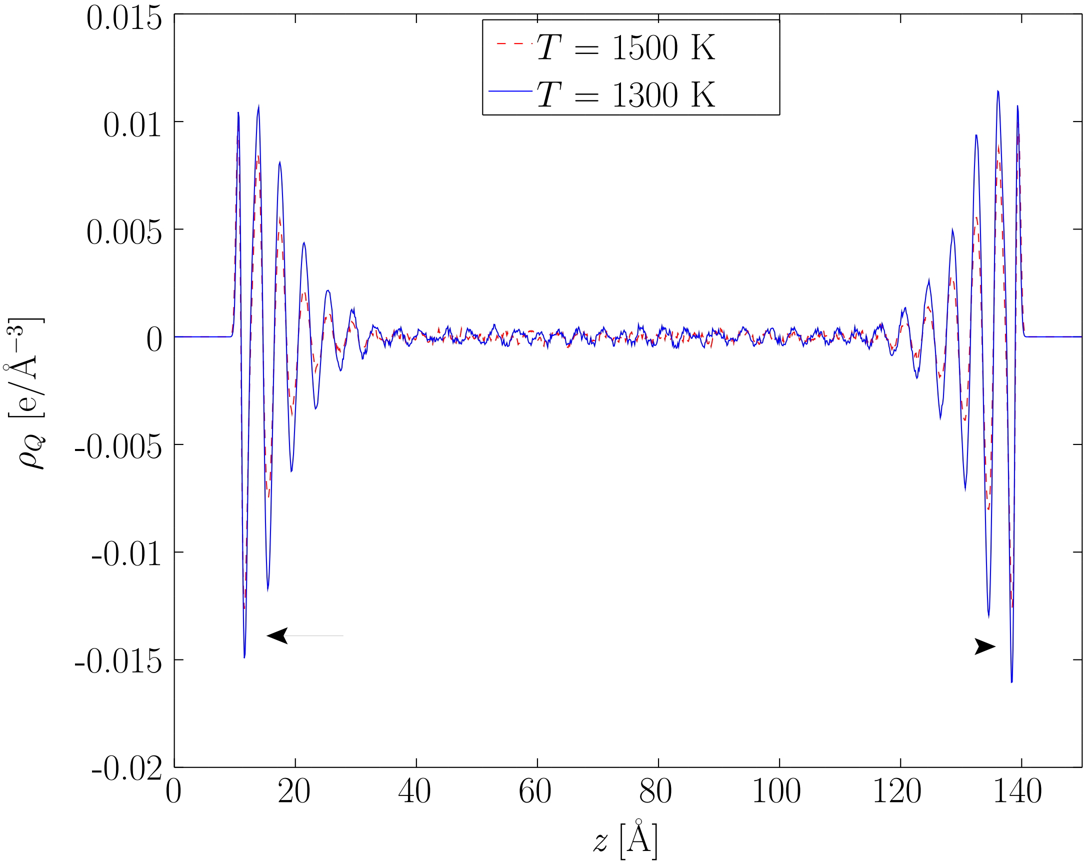

FIG. 9: Charge density profile for Li_2CO_3 confined between two planar neutral walls. Full line, blue: $T = 1300$ K. Dashed line, red: $T = 1500$ K. The two horizontal arrows point to the largest amplitude peaks in the charge density profile.

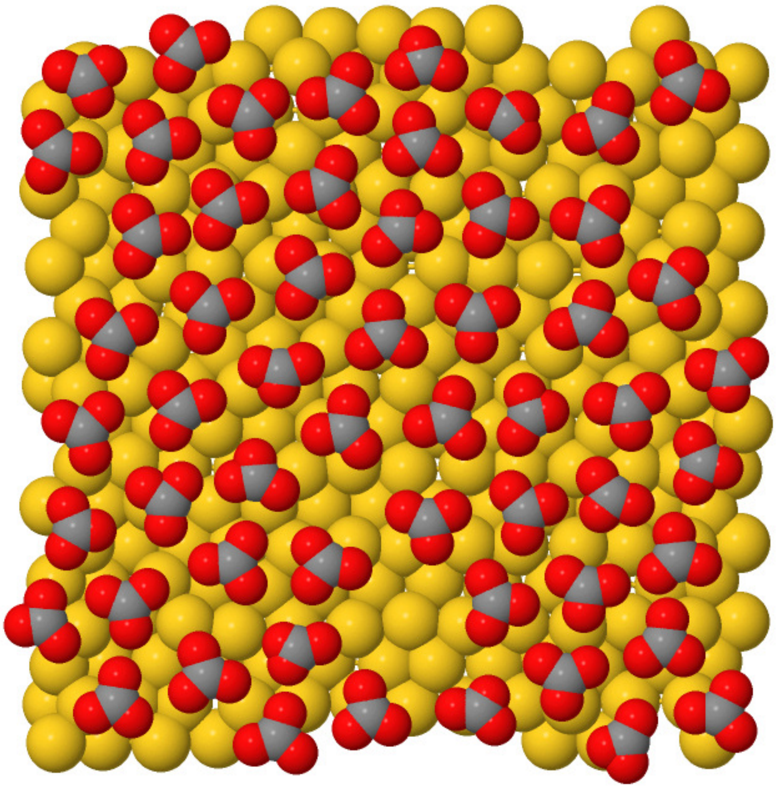

FIG. 10: Snapshot metal and CO_3^{2-} anions at the interface: yellow: metal (Au); red: oxygen; black: carbon. Li^+ cations are not shown. A CO_3^{2-} vacancy is apparent at the middle of the lower end.

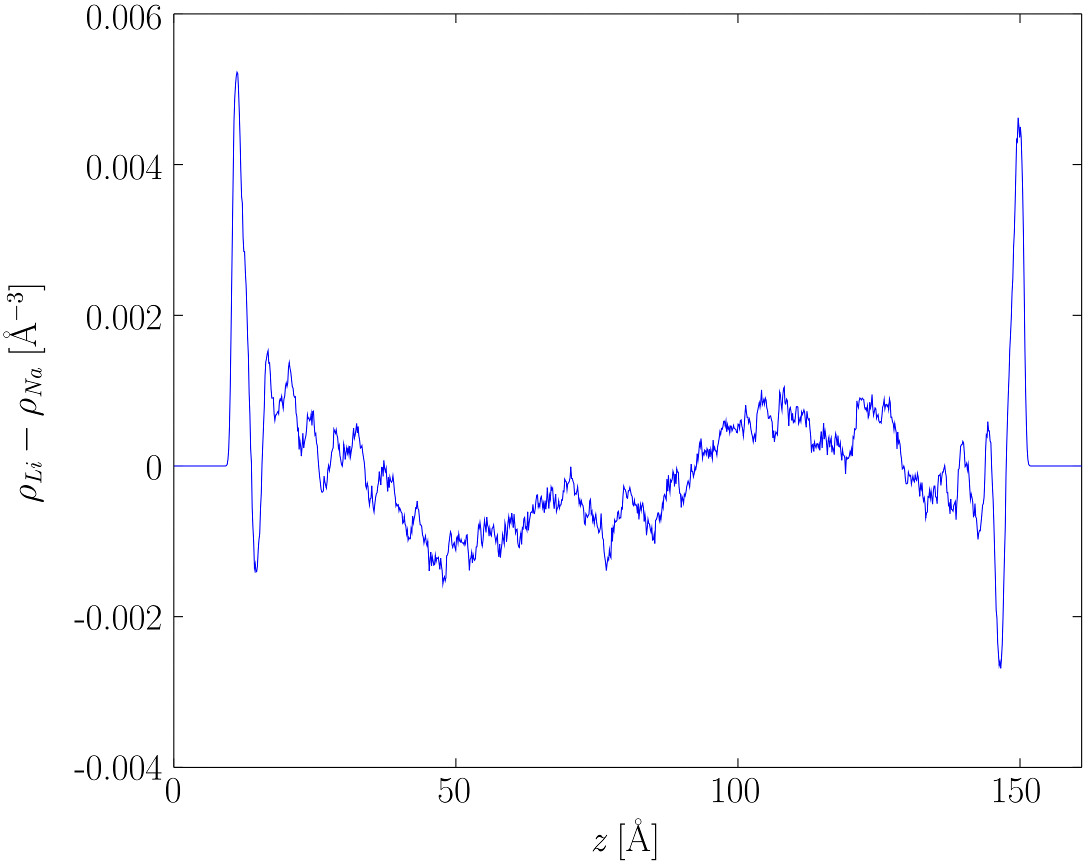

FIG. 11: Difference in the lithium and sodium number density in $\mathrm{LiNaCO_3}$ confined by two solid walls located at $z_a = ...$ and $z_b = ...$ i$T = 1300$ K.

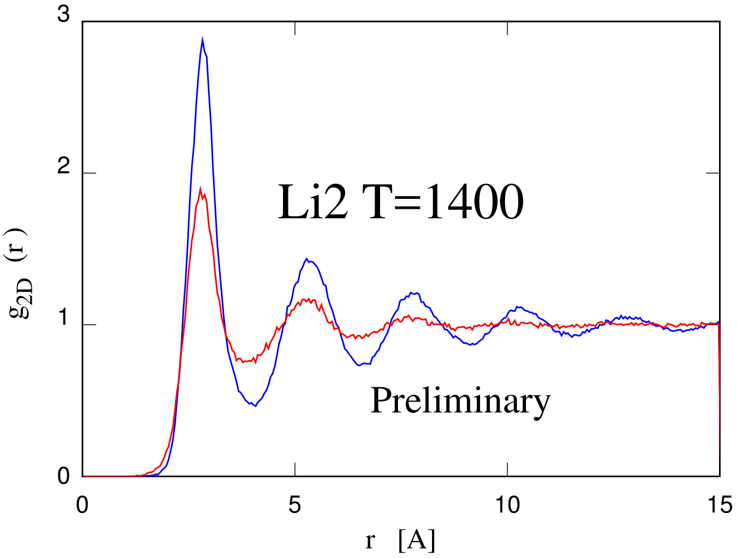

FIG. 12: Density correlations parallel to the surface in molten Li_2CO_3 confined by two solid walls located at $z_a = \ldots$ and $z_b = \ldots$. Blue line: next to the metal surface. Red line: in the bulk.

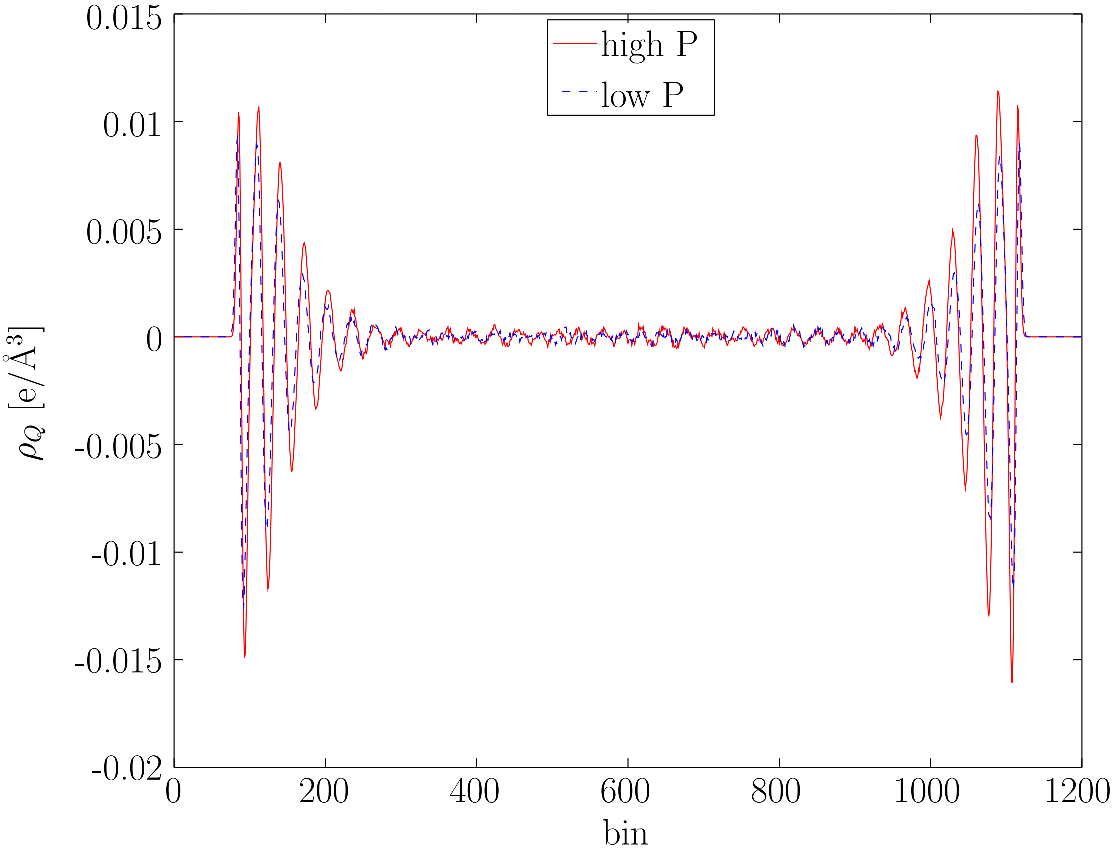

FIG. 13: Charge density profile for Li_2CO_3 at $T = 1300$ K for $P \approx 7$ kbar (dashed line, blue) and $P \approx 11$ kbar (full line, red).

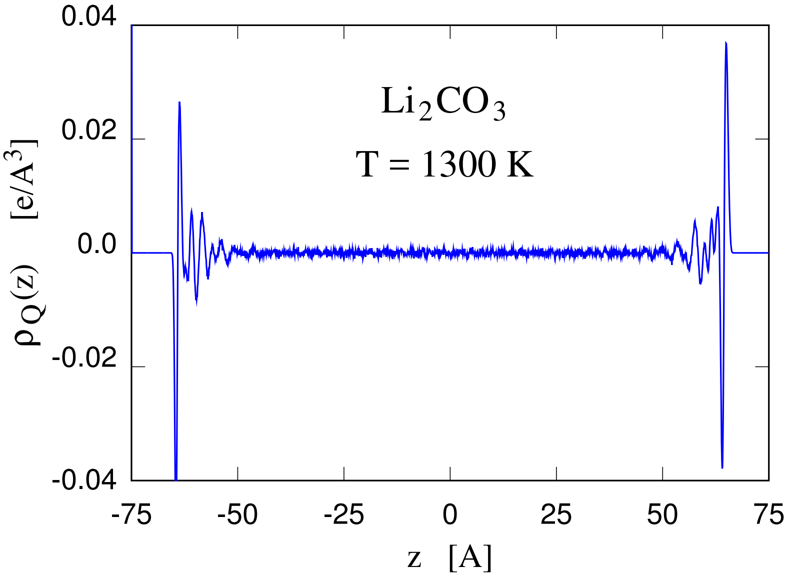

FIG. 14: Charge density profile in a molten $\mathrm{Li_2CO_3}$ slab confined between two walls of opposite surface charge density $\sigma = 0.07$ C/cm^2 at $z_A = -66$ Å , and $\sigma = -0.07$ C/cm^2 at $z_b = 66$ Å

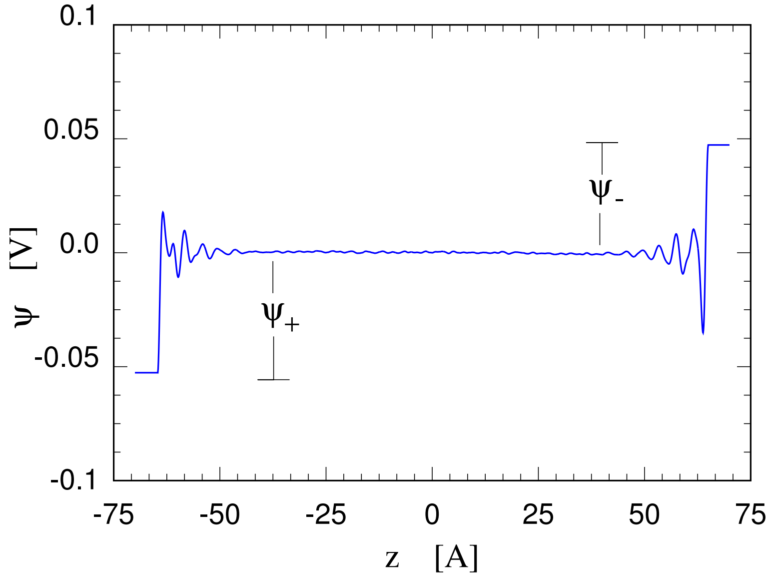

FIG. 15: Electrostatic potential across a molten Li_2CO_3 slab confined between two walls of opposite surface charge density $\sigma = 0.07$ C/cm^2 at $z_A = -66$ Å , and $\sigma = -0.07$ C/cm^2 at $z_b = 66$ Å .

Tables

TABLE I: Force field parameters used to model Li_2CO_3, Na_2CO_3 and K_2CO_3 using Eq. (1)[60].

Atom type	z [e]	n	σ [Å]
C	1.54	2.46	1.10
O	-1.18	7.18	1.33
Li	1.0	2.00	0.77
Na	1.0	8.00	1.07
K	1.0	8.00	1.39

TABLE II: Force field parameters used to model the harmonic bonds, angles and improper torsions in ${CO_3}^{2-}$.

Parameter	value
K_θ [kcal mol^{-1} rad^{-2}]	100.0
K_ϕ [kcal mol^{-1} rad^{-2}]	45.0
θ_0 [degrees]	120.0
ϕ_0 [degrees]	180.0

TABLE III: Lennard-Jones parameters for the atom species in M_2CO_3 from the OPLS force field model.

Species	σ_{ii} [Å]	ϵ_{ii} [ ]	
Li^+			
Na^+			
K^+			
C			
O			

TABLE IV: Nominal temperature (T_{nom}) and actual temperature ($\langle T \rangle$) and pressure ($\langle P \rangle$) for all simulations of homogeneous samples in the microcanonical ensemble. The volume per M_2CO_3 molecule (V_m) is reported as well. The nominal pressure is 15 kbar in all simulations. The statistical error is implicitly given by the number of digits in the quoted results. No attempt has been made to correct for deviations from the nominal temperature and pressure.

M_2CO_3	T_{nom} [K]	$\langle T \rangle$ [K]	$\langle P \rangle$ [bar]	V_m [Å^3]]
Li_2CO_3	1200	1207	15230	76.35
Li_2CO_3	1300	1295	13830	77.91
Li_2CO_3	1400	1406	15290	78.16
Li_2CO_3	1500	1492	13889	79.76
Na_2CO_3	1200	1192	15080	90.95
Na_2CO_3	1300	1320	15930	91.93
Na_2CO_3	1400	1390	14730	93.50
Na_2CO_3	1500	1494	15160	94.41
K_2CO_3	1200	1191	13640	125.11
K_2CO_3	1300	1302	15450	125.15
K_2CO_3	1400	1397	15070	127.03
K_2CO_3	1500	1494	13899	130.05
$LiNaCO_3$	1300	1318	15280	84.78

TABLE V: Average volume in Å ^{3} of the Voronoi polyhedra around each ion species in homogeneous M_2CO_3 molten alkali carbonates as a function of temperature. The volume for CO_3^{2-} is the sum of the volumes of its carbon and oxygen constituent atoms. The volume fraction of cations and anions is reported in parentheses on the following line. The statistical error bar affects the first decimal digit of absolute and relative volumes.

M_2CO_3	Ion	$T = 1200$ K	$T = 1300$ K	$T = 1400$ K	$T = 1500$ K
Li_2CO_3	Li^+	15.3	15.7	15.8	16.1
		(40.2)	(40.4)	(40.4)	(40.5)
	CO_3^{2-}	45.6	46.4	46.5	47.4
		(59.8)	(59.6)	(59.6)	(59.5)
Na_2CO_3	Na^+	19.15	19.4	19.8	20.0
		(42.2)	(42.2)	(42.3)	(42.4)
	CO_3^{2-}	52.6	53.1	53.9	54.3
		(57.8)	(57.8)	(57.7)	(57.6)
K_2CO_3	K^+	28.0	28.1	28.5	29.3

		(44.8)	(44.8)	(44.9)	(45.0)
	CO_3^{2-}	69.0	69.0	69.9	71.4
		(55.2)	(55.2)	(55.1)	(55.0)
$LaNaCO_3$	Li^+	-	15.6	-	-
			(18.4)		
	Na^+	-	19.4	-	-
			(22.9)		
	CO_3^{2-}	-	49.65	-	-
			(58.6)		

TABLE VI: Coordination number between the cation and oxygen at different target temperatures.

Type	T = 1200 K	T = 1300 K	T = 1400 K	T = 1500 K
n_{OLi}	4.0	3.9	3.9	3.9
n_{CLi}	3.9	3.9	3.9	3.9
n_{ONa}	5.1	5.1	5.0	5.0
n_{CNa}	4.3	4.3	4.3	4.3
n_{OK}	6.2	6.2	6.1	6.0
n_{CK}	4.5	4.5	4.5	4.5

TABLE VII: Transport properties for Li_2CO_3

T [K]	ρ [g/cm^3]	λ [W m^{-1}K^{-1}]	κ [S/cm]	κ_{NE} [S/cm]	D_{Li} [cm^2/s]	D_{CO_3} [cm^2/s]
1207	1.609	3.7 ± 0.2	4.1 ± 0.6	3.31	$(6.3 \pm 0.2) \times 10^{-5}$	$(9.7 \pm 1.3) \times 10^{-6}$
1295	1.577	4.0 ± 0.2	5.1 ± 0.6	3.91	$(8.0 \pm 0.2) \times 10^{-5}$	$(1.31 \pm 0.12) \times 10^{-5}$
1406	1.572	3.7 ± 0.2	5.7 ± 0.6	4.43	$(9.5 \pm 0.6) \times 10^{-5}$	$(1.81 \pm 0.09) \times 10^{-5}$
1492	1.540	3.7 ± 0.2	5.5 ± 0.6	5.16	$(1.2 \pm 0.3) \times 10^{-4}$	$(2.40 \pm 0.14) \times 10^{-5}$

TABLE VIII: Transport properties for Na_2CO_3

T [K]	ρ [g/cm^3]	λ [W m^{-1}K^{-1}]	κ [S/cm]	κ_{NE} [S/cm]	D_{Na} [cm^2/s]	D_{CO_3} [cm^2/s]
1192	1.937	0.94 ± 0.07	2.24 ± 0.11	2.03	$(3.8 \pm 0.3) \times 10^{-5}$	$(9.4 \pm 1.1) \times 10^{-6}$

1320	1.916	0.98 ± 0.07	2.74 ± 0.11	2.35	$(5.02 \pm 0.09) \times 10^{-5}$	$(1.26 \pm 0.04) \times 10^{-5}$
1390	1.884	0.95 ± 0.07	2.90 ± 0.11	2.66	$(5.8 \pm 0.3) \times 10^{-5}$	$(1.56 \pm 0.16) \times 10^{-5}$
1494	1.866	0.93 ± 0.07	3.31 ± 0.11	2.99	$(7.37 \pm 0.06) \times 10^{-5}$	$(2.12 \pm 0.14) \times 10^{-5}$

TABLE IX: Transport properties for K_2CO_3

T [K]	ρ [g/cm^3]	λ [W m^{-1} K^{-1}]	κ [S/cm]	κ_{NE} [S/cm]	D_K [cm^2/s]	D_{CO_3} [cm^2/s]
1191	1.836	0.98 ± 0.06	1.24 ± 0.15	1.06	$(2.60 \pm 0.14) \times 10^{-5}$	$(8.2 \pm 0.3) \times 10^{-6}$
1302	1.835	0.87 ± 0.06	1.32 ± 0.15	1.29	$(3.5 \pm 0.3) \times 10^{-5}$	$(1.13 \pm 0.09) \times 10^{-5}$
1397	1.808	0.91 ± 0.06	1.61 ± 0.15	1.49	$(4.34 \pm 0.14) \times 10^{-5}$	$(1.53 \pm 0.05) \times 10^{-5}$
1494	1.766	0.94 ± 0.06	2.17 ± 0.15	1.77	$(5.49 \pm 0.18) \times 10^{-5}$	$(1.88 \pm 0.14) \times 10^{-5}$

TABLE X: Thermodynamic width W_l of the molten carbonate layer consisting of $N_{mol} = 2048$ M_2CO_3 molecules. Data available but to check.

M_2CO_3	$T = 1300$	$T = 1400$	$T = 1500$
Li_2CO_3	130.2	130.2	130.25
Na_2CO_3	149.6	151.6	-
K_2CO_3			
$LiNaCO_3$			

TABLE XI: Characteristic time (ps) for ions hopping out of the first density layer in contact with the solid wall (see text).

M_2CO_3	$T = 1300$	$T = 1400$	$T = 1500$
Li^+ in Li_2CO_3	11.3	7.7	6.6
CO_3^{2-} in Li_2CO_3	36.7	28.7	28.4
Na^+ in Na_2CO_3	14.0	-	-
CO_3^{2-} in Na_2CO_3	66.4	-	-
K^+ in K_2CO_3	12.9	-	-
CO_3^{2-} in K_2CO_3	15.0	-	-

TABLE XII: Average pressure in the liquid phase of molten carbonate sample confined between two neutral solid walls.

System	P (1300 K) [kbar]	P (1400 K) [kbar]	P (1500 K) [kbar]
Li_2CO_3	11.0	13.7	16.3
Li_2CO_3 (area × 2)	11.0	-	-
Li_2CO_3 (area × 4)	11.0	-	-
$LiNaCO_3$	13.0	-	-
Na_2CO_3	18.2	18.6	-
K_2CO_3	17.9	14.2	-

TABLE XIII: Interfacial dipole at different temperatures for different systems.

System	D (1300 K) [D/nm^2]	D (1400 K) [D/nm^2]	D (1500 K) [D/nm^2]
Li_2CO_3	2.56 ± 0.07	2.66 ± 0.08	2.73 ± 0.08
Li_2CO_3 (area × 2)	2.69 ± 0.06	-	-
Li_2CO_3 (area × 4)	2.72 ± 0.05	-	-
$LiNaCO_3$	2.56 ± 0.09	-	-
Na_2CO_3	2.39 ± 0.12	2.42 ± 0.06	-
K_2CO_3	1.77 ± 0.06	1.84 ± 0.06	-

TABLE XIV: Interfacial capacitance (μF/cm^2) at different temperatures for different systems.

System	Li_2CO_3	Li_2CO_3	Li_2CO_3	Na_2CO_3	K_2CO_3
T (K)	1300	1400	1500	1300	
C_D μF/cm^2	24 ± 0.5	27 ± 0.6	29 ± 0.6	22 ± 0.8	17 ± 0.7